İSTANBUL TECHNICAL UNIVERSITY ★ INSTITUTE OF SCIENCE AND TECHNOLOGY

MOTOR CONTROL VIA WIRELESS ENERGY AND INFORMATION TRANSFER

M.Sc. Thesis by

Utku KARAKAYA, B.Sc.

Department : Mechatronics Engineering

Programme: Mechatronics Engineering

SEPTEMBER 2007

İSTANBUL TECHNICAL UNIVERSITY ★ INSTITUTE OF SCIENCE AND TECHNOLOGY

MOTOR CONTROL VIA WIRELESS ENERGY AND INFORMATION TRANSFER

M.Sc. Thesis by

Utku KARAKAYA, B.Sc.

518041019

Date of submission : 11 September 2007

Date of defence examination: 14 September 2007

Supervisor (Chairman): Assist. Prof. Dr. Özgür ÜSTÜN

Members of the Examining Committee Prof. Dr. M. Sait TÜRKÖZ

Assoc. Prof. Dr. Ata MUĞAN

SEPTEMBER 2007

İSTANBUL TEKNİK ÜNİVERSİTESİ ★ FEN BİLİMLERİ ENSTİTÜSÜ

KABLOSUZ ENERJİ VE BİLGİ TRANSFERİ İLE MOTOR KONTROLÜ

YÜKSEK LİSANS TEZİ

Müh. Utku KARAKAYA
518041019

Tezin Enstitüye Verildiği Tarih : 11 Eylül 2007
Tezin Savunulduğu Tarih : 14 Eylül 2007

Tez Danışmanı : Yrd. Doç.Dr. Özgür ÜSTÜN
Diğer Jüri Üyeleri Prof.Dr. M. Sait TÜRKÖZ
Doç Dr. Ata MUĞAN

EYLÜL 2007

ACKNOWLEDEGEMENT

First of all, I would like express my gratitude to my supervisor Assist. Prof. Özgür ÜSTÜN, not only for his support but also for giving me the opportunity to realize my thesis at Mekatro R&D.

I, also, would like to thank Prof. Nejat TUNCAY, whom encouraged me to start this thesis, for his support at Mekatro R&D.

I would like to thank Talat, Murat and Sedat YENİYURT and Bülent SİNANOĞLU from Yeniyurt Gear and Machinery Co. LTD. As a mechatronics engineer, I had the chance to practice in mechanics by their ultimate support.

I wish to thank to my colleague Mert ÇİFTÇİOĞLU, especially for his help during construction of the mechanical parts.

I would like to thank Murat ŞEHİRLİOĞLU for teaching me many practical aspects of electronics. Also, I wish to thank Utku ALTUNKAYA for his support in software issues.

I would like to thank to Deniz PAZARCI from Yeditepe University. She has always encouraged me through this thesis and in electronics since the 'Introduction to Electronics' course. She has been a teacher, a colleague and a friend to me.

And last but not least, I wish to thank to my family, mum, dad, my brother for their infinite support, thrust and love. Also, I am very thankful to my grandmother, for her patience to me thorough all these years.

September 2007 Utku KARAKAYA

CONTENTS

LIST OF ABBREVIATIONS

ESR	: Equivalent Series Resistance
FSK	: Frequency Shift Keying
ASK	: Amplitude Shift Keying
EMC	: Electromagnetic Compatibility
RLC	: Resistor-Inductor-Capacitor
AC	: Alternating Current
DC	: Direct Current
MOSFET	: Metal Oxide Semiconductor Field Effect Transistor
FEA	: Finite Element Analysis
PWM	: Pulse Width Modulation
LCD	: Liquid Crystal Display
OPAMP	: Operational Amplifier
CAD	: Computer Aided Design
ISO	: International Standards Organization

LIST OF TABLES

LIST OF FIGURES

LIST OF SYMBOLS

L_P : Primary leakage inductance
L_S : Secondary leakage inductance
C_P : Primary resonance capacitor
C_S : Secondary resonance capacitor
M : Mutual inductance between primary and secondary coils
k : Coefficient of coupling
ω : frequency in rad/sec
f : frequency in 1/sec
Z_S : Secondary impedance
Z_L : Secondary load
R_S : Secondary winding resistance
R_P : Primary winding resistance
N : Number of turns of a coil
Φ : Magnetic flux
μ : permeability
σ : conductivity

KABLOSUZ ENERJİ VE BİLGİ TRANSFERİ İLE MOTOR KONTROLÜ

ÖZET

Bu tezde amaç, kablosuz enerji ve bilgi iletimi ile motor kontrolü yapmaktır. Aralarında enerji transferi yapılan birincil ve ikincil sistemler arası mesafe yaklaşık 10mm'dir. İkincil tarafda bir DC motora, vidalı bir mekanik sistem monte edilerek doğrusal hareket elde edilmiştir. Birincil sistem, ikincil sisteme kablosuz olarak enerji göndermektedir. Aynı zaman da, gönderilen güç sinyalinin içine motorun hangi yönde ve ne kadar döneceğini bildiren bilgi mesajı da eklenmiştir. İkincil sisteme gönderilen güç 0.5W ile 3W arasında olacak şekilde tasarlanmıştır.

Ansoft Maxwell 3D ve OrCAD PSpice simulasyon programları ile tasarlanan iki adet bobin arasında kurulan manyetik kuplaj ile enerji gönderimi istenen mertebelerde sağlanmıştır. Bunun için yarım köprü devresi sürülen rezonans devresi kullanılmış, ve kaçak endüktanslar bastırılmıştır. Kurulan test devreleri üzerinde yapılan ölçümler ve simulasyon sonuçları arasındaki örtüşme öngörülen modellememin doğruluğunu göstermiştir. Enerji iletiminde ise %60 verime kadar çıkılmıştır.

Bilgi transferi için, donanım yerine yazılım esaslı yeni bir yöntem önerilmiş gerçeklenmiştir. Asenkron yarı dubleks bilgi transferi ile 1.6 kbit/s hızlara kadar çıkılmıştır.

Mekanik sistem, bir DC motor, bir yüksek oranlı dişli kutusu ve M10x1 standartında diş açılmış vidadan oluşmaktadır. Sistemin mekanik çözünürlüğü 0.1221 µm civarındadır. Konum kontrolü için motor üzerine bir adet enkoder eklenmiştir. İkincil kısımdaki mikrodenetleyici, enkoderden gelen bilgiye gore motoru doğrusal konumlama için sürmektedir.

MOTOR CONTROL VIA WIRELESS ENERGY AND INFORMATION TRANSFER

ABSTRACT

The aim of this thesis is to control a DC motor by means of wireless transfer of energy and information. Separation between primary and secondary system is about 10mm. At the secondary side, a DC motor is connected to lead screw mechanism that provides translational motion. Primary system sends energy to the secondary system. At the same time it sends displacement and direction data, which is embedded into the transmitted power signal. Power delivered to the secondary side is between 0.5W and 3W.

Through the thesis, by employing Ansoft Maxwell 3D and OrCAD PSpice programs two magnetically coupled coils are designed, and succeeded to transfer energy in required levels. Drive circuit designed as half bridge resonant tank in order to cancel the leakage inductances. Correlation between measurements on the test circuits and simulation results clearly implies that proposed models are valid. System achieved efficiencies up to 60%.

For information transfer, a new method based on the software technique is proposed and realized. A half duplex asynchronous data transfer is achieved up to 1.6 kbits/s.

The mechanical system constructed by using a DC motor, a high ratio planetary gear box and M10x1 lead screw. System has a resolution of 0.1221μm. An incremental encoder is mounted on the motor for position control. A microcontroller at the secondary side runs motor for linear positioning depending on the feedback from encoder.

1. INTRODUCTION

The most convenient way of transferring energy and information has always been by means of wires and plugs. In recent years, wireless communication has become an opponent of data transmission by wire. When dealing with energy transfer, transmission by wire is significantly dominant, due to its simplicity, reliability and high efficiency. However, in some mediums wires cause more problems than they solve. Such as at underwater facilities, it is not possible to use plugs as the medium is conductive. When using body implants, such as artificial heart, wires that pass through the skin may cause health issues, like inflammation. Some consumer electronics companies provide washable products such as shaving machines in which it is not safe to use plugs or wires for energy transfer. In view of these constraints, wireless energy transfer systems can be used in expense of decreased efficiency and additional costs due to use of electronic systems.

In addition to energy transfer, information transfer can also be embedded in energy signal by employing electronic systems. Data links enable controlling systems while powering them. Depending on the requirements of the system, information transfer can be unidirectional or bidirectional.

The systems that transfer energy to body implants are called transcutaneous systems. Such systems are required especially for artificial hearts, pacemakers, cochlear implants and orthopaedic implants [1]. Data link is sometimes required to get information about condition of the implant, or to control it properly.

The aim of this thesis is develop a system for body implants which is capable of driving and controlling a DC motor by wireless energy and information transfer. The DC motor is connected to a lead screw mechanism, which converts rotational motion to translational motion with a resolution of 0.1221 μmeters.

Through the thesis, an overview of the system will be introduced, including design elements and constraints. After that a wireless energy transfer scheme will be proposed. Then an information transfer topology will be added into the energy transfer scheme. Later, a mechanical system will be designed providing linear motion

by a DC motor. Based on the designed systems, electronic and mechanical systems will be manufactured to realize them. At the end overall system performance will be evaluated comparing results with realized electronic and mechanical systems.

1.1. Overview of the system

In order to transfer energy wirelessly, two magnetically coupled coils are used. Basically these coils resemble transformers that have very low coupling coefficient. Primary coil injects power to the secondary coil, and is placed just above the skin. Secondary coil is placed about 10 mm under the skin. At Figure 1.1, schematic overview of the system is depicted. When a time varying signal is applied to the primary coil, a magnetic field is created around the coil. Time varying magnetic field induces current in the secondary coil. Primary drive system includes a power stage to drive coil and microcontroller stage to control power stage, to send and receive data. Secondary part consists of rectifier, regulator stages, motor drive stage and finally a microcontroller to control them.

The power link can also be used for data link for transmitting information by using FSK, ASK, or other communication techniques. Depending on the information received from primary system, secondary system drives the motor in the requested direction by getting feedback from incremental encoder.

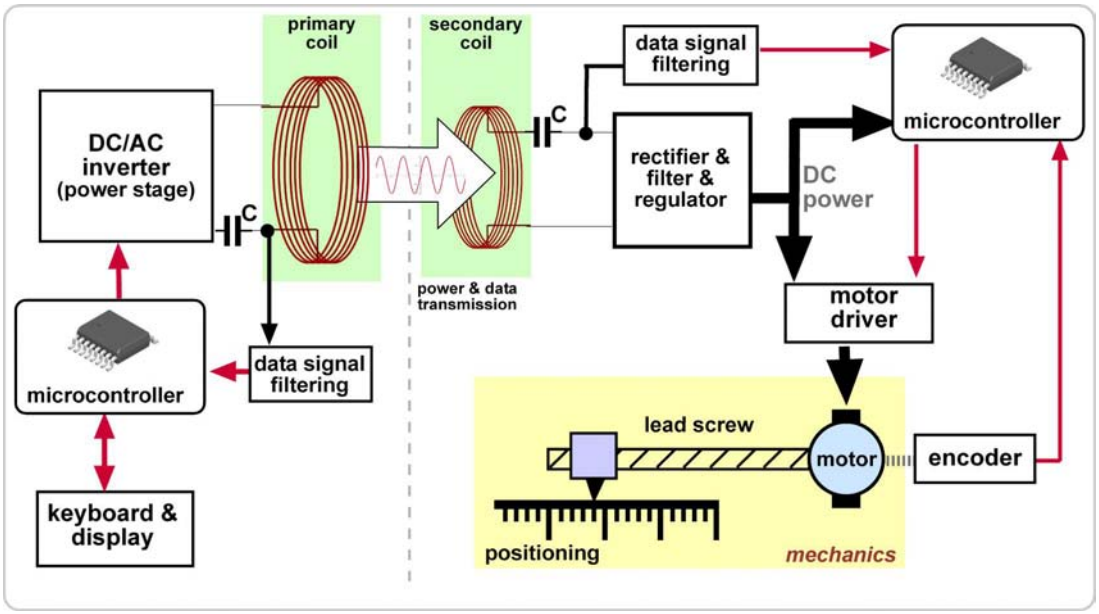

Figure 1.1: Schematic overview of the system

The separation between coil is depends on the application and may vary from a few millimetres to several centimetres. Usually, it is about 8-12mm. Because of the relatively large separation, coils are loosely coupled, about 10%-30%. That's why efficiency of the system is low. As the coupling decreases, more power is required to induce same power at the secondary coil [2].

Considering the magnetic waves penetrating into the skin, one would ask its effects on the human tissue. Researches have revealed that there is not a significant effect on the tissues [3]. At [4], a 40W transcutaneous energy system is shown to be below the absorption rate limits of tissue. Also, thermal effects caused by electromagnetic waves are insignificant.

1.2. Design constraints

It is important to clearly define design constraints as the whole system will be constructed on these limitations. In addition, optimization will be done according to design constraints.

First of all, implanted device should not disturb the patient. The less he feels it under the skin, the more he feels comfortable. So, secondary coil and circuit should be as small as possible [5]. If the receiver coil is placed very close to skin surface, the patient will be disturbed by it. There should be a distance between skin surface and coil. On the other hand, if the distance is too high, patient would have problems while aligning primary and secondary coils. A higher distance would also cause decreased coupling between coils, resulting in decreased efficiency. There is a trade-off when determining skin-coil distance. Approximately 10mm seems fair for this application [6].

Transmitter coil and receiver coil are totally independent parts. While the patients using it, there may be some deviations in the horizontal and angular alignments of the coils. Displacement of the coils is also another deviation. Figure 1.2 shows possible deviations while matching the coils. Most significant effect of these deviations is the variation in the coefficient of coupling. It directly effects efficiency and delivered power. Regardless of how careful the patient is, there will always be some deviation. So the system should be immune to any change in the coefficient of coupling [5].

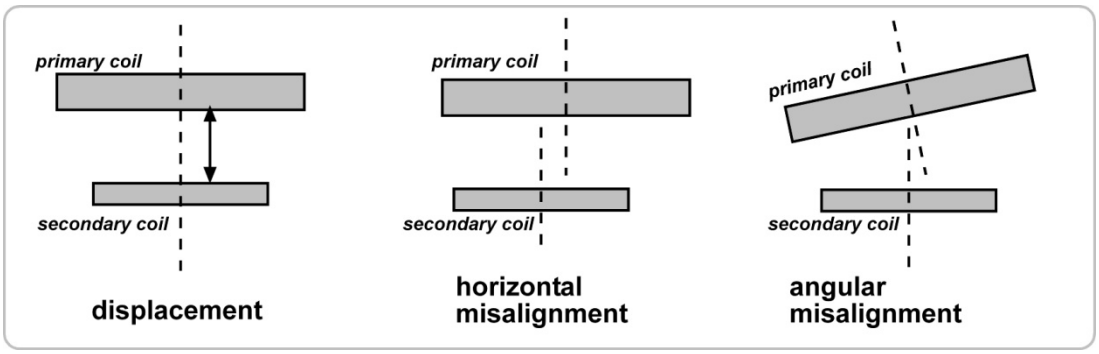

Figure 1.2: Deviation in the alignment, orientation, and distance of the coils

Secondary system will control the motor according to sent data from primary. If the received data distorted and the secondary system does not recognize it, motor would run in a wrong way causing serious problems. Data transmission system should be reliable and able to check the validity of the received data.

Receiver circuit is placed into the body by a surgical operation. So it should be very reliable and robust as it is always risky for a patient to go through a surgery.

The power of the motor that will be driven is 1.3 W. Including microcontroller power, motor encoder power; rectifier and regulator losses, total power requirement of the receiver system can be up to 3W. When the motor is not running then the required power will be approximately 0.5W. The system should be able to cover all power range of the receiver. This condition requires immunity to variation in the load.

Created magnetic fields by coils may conflict with electromagnetic compatibility (EMC) limits [7]. If required, precautions should be taken to minimize the radiated magnetic field.

In addition to these requirements, it would be practical to design the transmitter as a portable device. A battery operated handheld device would be preferable.

Also, end user would not be familiar to electronic devices. So user interface should be as simple as possible. System should be self adjusting for leaving less control to the user.

2. WIRELESS TRANSFER OF ENERGY

The most challenging part of the system is designing an efficient energy transfer system. As mentioned previously, coils behave like air core transformers. However, they cannot be characterized by turn ratios like conventional transformers as they are loosely coupled. The separation between coils decreases coefficient of coupling significantly. Loose coupling also causes an increase at leakage inductances, which considerably decrease efficiency. In view of these issues, topologies that incorporate the leakage inductance into circuit operation are used [8].

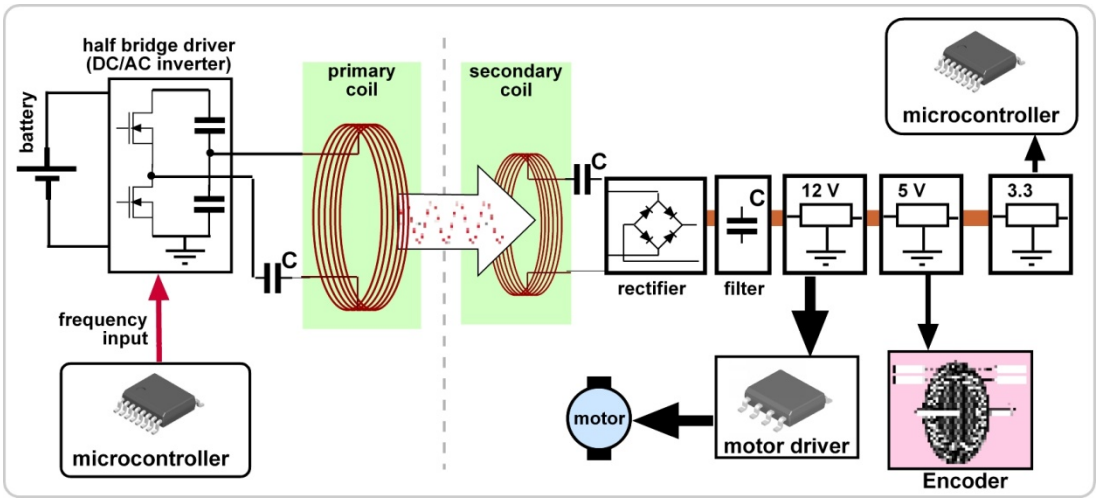

Figure 2.1: Energy Transfer scheme

2.1. Modelling magnetically coupled coils

Self and mutual inductances are used for modelling magnetically coupled coils. Figure 2.2 shows schematic view of magnetically coupled coils, where L_P and L_S are self inductances of primary and secondary, respectively. These coils are related to each other by a mutual inductance M. Equations for the coupled inductance are [9],

$$v_p = L_p \frac{di_p}{dt} + M \frac{di_s}{dt} \tag{2.1}$$

$$v_s = M\frac{di_p}{dt} + L_s\frac{di_s}{dt} \tag{2.2}$$

These equations clearly imply that any magnetic flux created in of the coils links the companion coil depending on the value of the mutual inductance (M). The degree of the linkage is defined by the coefficient of coupling (k), which is,

$$k = \frac{M}{\sqrt{L_p L_s}} \tag{2.3}$$

Coefficient of coupling does not have a unit. As the mutual inductance increases, coefficient of coupling increases. For an ideal transformer k is equal to unity, which means they are perfectly coupled. In real transformers coupling is about 0.99 (99 %). In this thesis, coupling is relatively low, such as 0.1 or 0.2. Calculation of coupling will be explained in later sections.

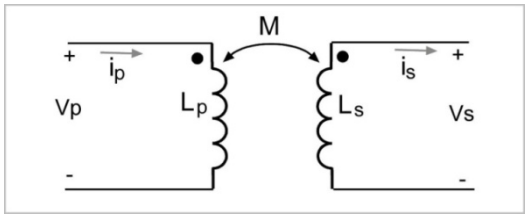

Figure 2.2: Magnetically coupled coils

Referring to the previous coupling model, source and load can be added to system to create a basic circuitry of the energy transfer system. Figure 2.3 shows schematic view of coils where primary coil is driven by sinusoidal voltage source. Z_S is impedance of source and Z_L is impedance of the load at the receiver part. R_P and R_S are winding resistance of primary and secondary coils, respectively. Receiver part is implanted under the skin and linked to the primary by mutual inductance.

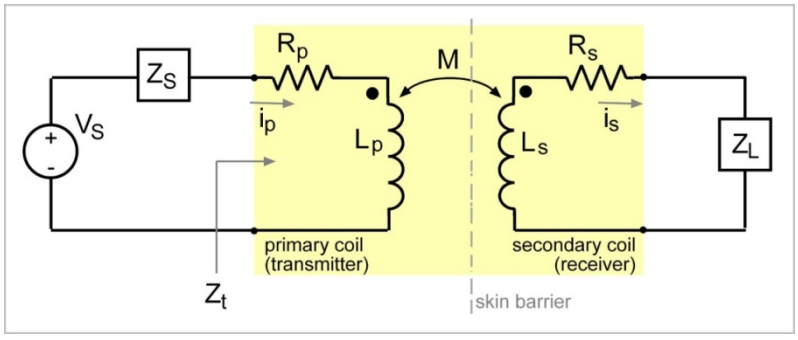

Figure 2.3: Magnetically coupled coils

Depending on the amount of mutual inductance (so is the coupling), impedance of secondary side is reflected to primary side. So the total impedance that V_S faces includes not only self impedance of primary coil, but also the reflected impedance of secondary coil. In order to find total impedance that appears at the primary side, Z_T, mesh-current equation can be derived,

$$V_S = (Z_S + R_P + j\omega L_P)I_P - j\omega M I_s \tag{2.4}$$

$$0 = -j\omega M I_P + (R_S + j\omega L_S + Z_L)I_S \tag{2.5}$$

Total impedance that V_S sees is derived as [9],

$$Z_t = R_P + Z_S + j\omega L_P + \left[\frac{\omega^2 M^2}{R_S + j\omega L_S + Z_L}\right] \tag{2.6}$$

In this equation, the part, which is in brackets, is the reflected impedance of the secondary coil. This equation clearly implies that reactance part of impedance is highly dominant.

2.2. The Resonance

Before introducing resonant topology into the circuit at the previous section, it would be practical to explain resonance. At Figure 2.4, there is a basic resonant circuit which consists of serially connected resistance, capacitance and inductance. These elements are driven by AC voltage source whose frequency is ω. The total impedance that V_S see is,

$$Z_T = R + j\omega L - j\frac{1}{\omega C} = R + j\left(\frac{\omega^2 LC - 1}{\omega C}\right) \tag{2.7}$$

As an example, suppose that R=10Ω, L=100μH and C=10nF. If ω is swept from 750MHz to 1.3GHz, magnitude of Z_R varies as seen at Figure 2.5.

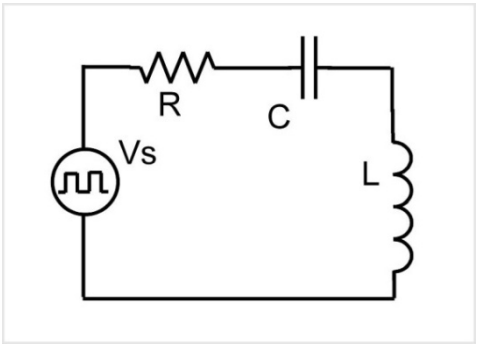

Figure 2.4: Basic resonance circuit

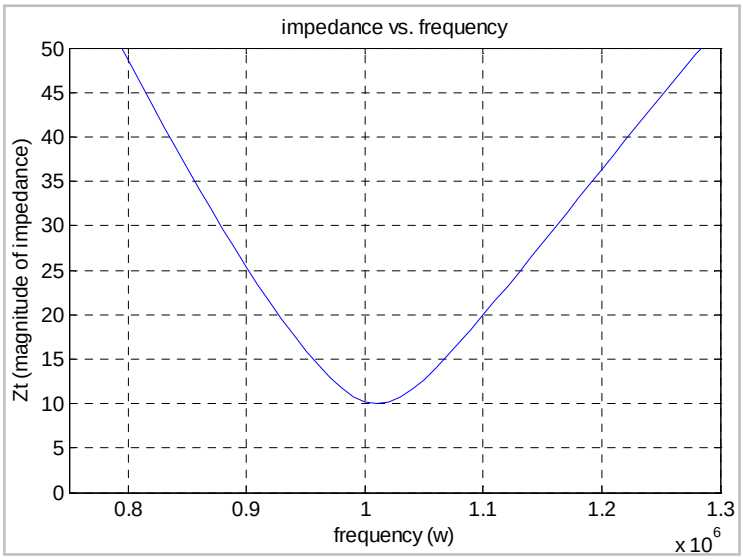

Figure 2.5: Impedance vs. frequency

At the point where ω is about 1 GHz, Z_T gives the minimum impedance. Minimum value of Z_T is 10Ω, which is value of the resistance at the circuit. So the RLC circuit acts like a pure resistance. The frequency, where impedance becomes pure resistance, is the resonant frequency of the RLC circuit. Above this frequency RLC exhibits inductive impedance, and below this frequency it exhibits capacitive impedance. The frequency, which makes reactive part of impedance zero, is,

$$\omega_r = \frac{1}{\sqrt{LC}} \qquad (2.8)$$

It is called the resonant frequency of the RLC circuit. The gain depends on the frequency. If the magnitude of the applied AC voltage is 10V, then current gain will vary by frequency, as shown at Figure 2.6.

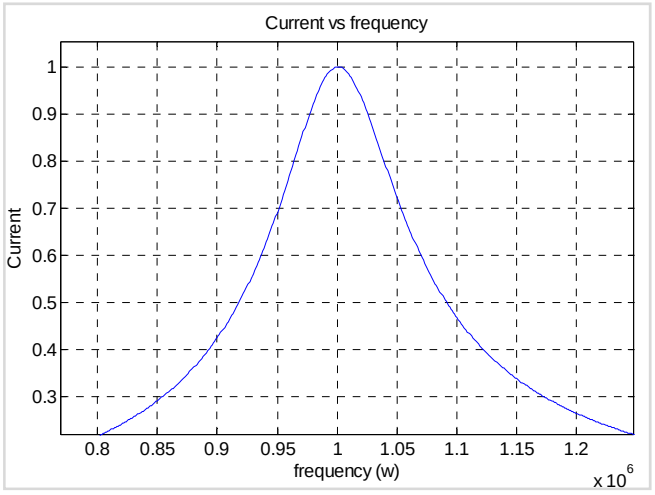

Figure 2.6: Current gain vs. frequency

Briefly, for resonant circuits, any reactive element can be cancelled by adding another reactive element that has equal impedance with opposite sign. This feature of resonant converters can be applied to wireless energy transformer for cancelling leakage inductances. To illuminate the effects of resonance applied to wireless energy transfer, conventional transformer can be used. At Figure 2.7, a transformer model and its equivalent circuit is shown. Also, C_p and C_s are added to provide resonance feature.

For conventional transformers, leakage inductance of both primary ($L_{p.leakage}$) and secondary ($L_{s.leakage}$) sides are very low compared to magnetizing inductance (L_{mag}). Thus, a great deal of the current flows to the secondary side through leakage inductances, as seen at equivalent circuit model. However, this is not true for air gap coils. Different from conventional transformers, the large air gap between coils, results in very large leakage inductances at both primary and secondary coils. In addition, large leakage inductance at the primary side will cause very low magnetizing inductance and hence increased magnetizing currents [10]. Due to low magnetizing inductance and large leakage inductance, a great portion of the current at the primary side will flow through the magnetizing inductance and go back to source. This circulating current will increase both conduction (I^2R) losses and component stress [8]. In order to alleviate problems associated with inductances, resonant capacitors can be added to the circuit. At Figure 2.7, C_p-$L_{p.leakage}$ and C_s-$L_{s.leakage}$ are resonant tanks. Near resonance frequency, they have very low impedance. At resonant frequency, these tanks act as pure resistance by totally cancelling reactance.

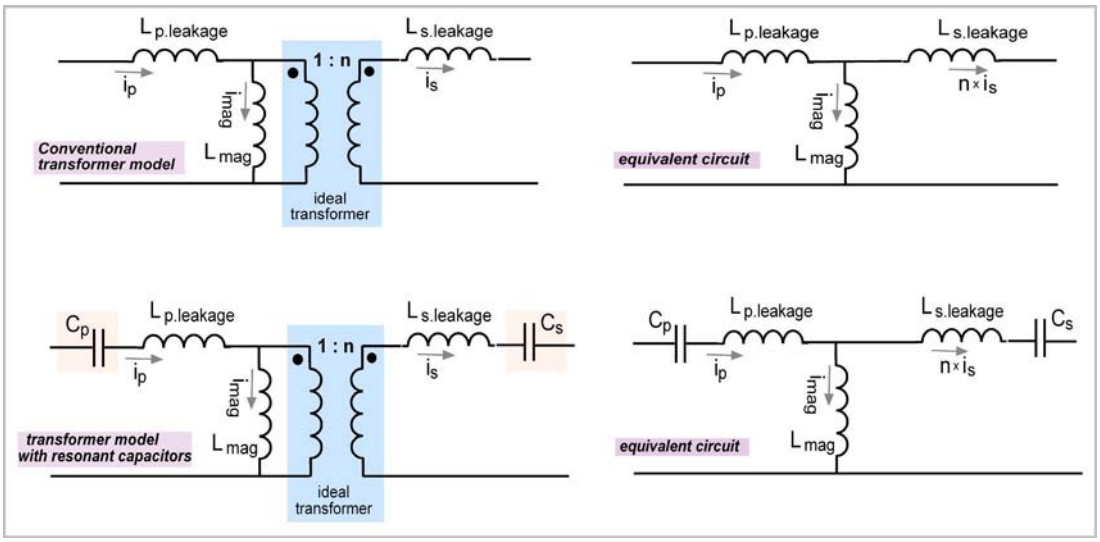

Figure 2.7: Conventional transformer model and equivalent circuit

In addition, resulting voltage and current signals across the inductors are almost pure sinusoidal signals; despite the applied voltage is a square wave. The most important advantage of sinusoidal wave is that electromagnetic radiation will be only at the applied frequency. If the inductor radiated square wave signals, then there would be many sinusoidal signals radiated at different frequencies of spectrum due to harmonics of square waves. Consequently, the possibility of electromagnetic interference would increase. Figure 2.8 shows resulting sine wave across the inductor when a square wave applied to resonant tank.

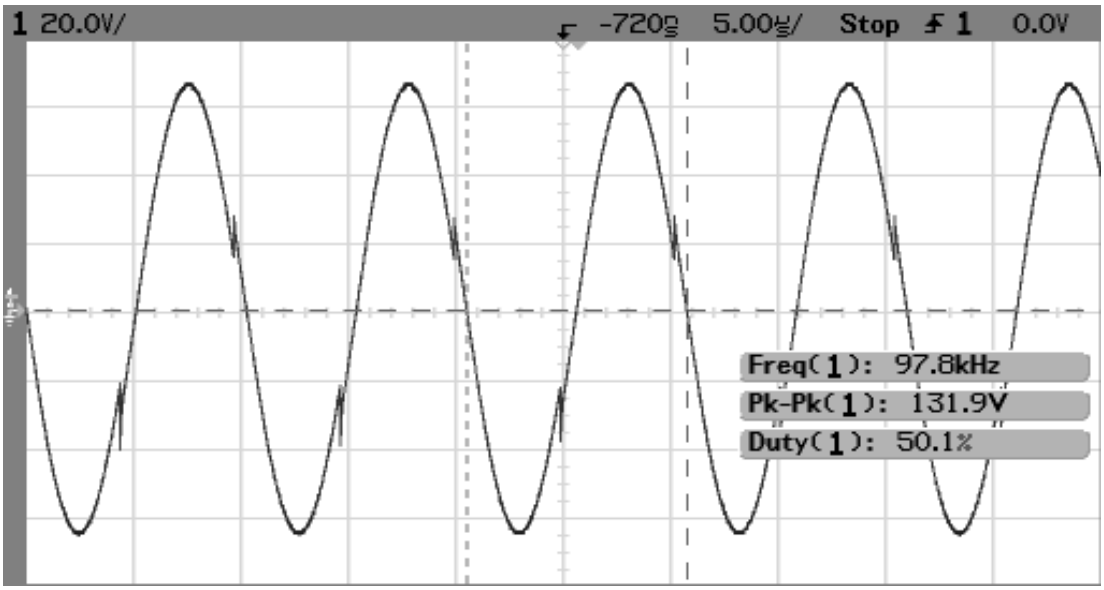

Figure 2.8: Resonant tank driving voltage and resulting voltage

Another advantage of resonance is that it decreases component stress during switching of MOSFETs. Without LC resonant circuits, switching devices are turned on and turned off at the load current which causes high *di/dt* values. Thus MOSFETs are subject high voltage stresses. During turn on and turn off, switching losses increase by frequency. High *di/dt* and *dv/dt* values would also cause electromagnetic interference [11].

Until now, advantages of resonance have been clarified. Now, resonance feature can be added to equation (2.6) to evaluate the results of resonance. If series C_p and C_s capacitors are placed in the circuit at Figure 2.3, equation (2.6) becomes,

$$Z_t = R_P + Z_S + j\omega L_P - \frac{j}{\omega C_P} + \left[\frac{\omega^2 M^2}{R_S + j\omega L_S - j/\omega C_S + Z_L} \right] \tag{2.9}$$

By rearranging terms, equation becomes,

$$Z_t = R_P + Z_S + j\frac{(\omega^2 L_P C_P - 1)}{\omega C_P} + \left[\frac{\omega^2 M^2}{R_S + Z_L + j\frac{(\omega^2 L_S C_S - 1)}{\omega C_S}} \right] \tag{2.10}$$

In this equation there are two resonant frequencies, one for primary side and other for secondary side. If secondary load Z_L is pure resistance, and if both resonant frequencies are tuned to same frequency, then resulting total impedance is pure resistance. Thus, there will be no reactive component causing circulating currents. Conduction losses will be alleviated. However, it is not always possible to keep system at resonance. Because any change in system would alter resonance frequency, such as change of temperature, change of mutual inductance. Also, switching to non resonant frequency, changes the gain of the resonant tank. So, it is possible to change frequency deliberately in order to adjust the power delivered to secondary.

2.3. Design Issues of Coils

While designing coils, there many parameters that should be considered, including their geometry, structures, inductances, winding resistance, coupling etc. Geometric approach would be the first step in coil design. Once the dimensions of the receiver and transmitter coils are determined, the rest of the design can be based on them.

Outer diameter of the coil expected to be less then 25mm [6]. It would be also practical to keep the coil thickness between 1mm and 3mm. Despite smaller diameters are preferred, there is a trade-off between coil diameter and induced voltage across the winding terminals. Neglecting the winding resistance, induced voltage at a coil defined in below equation,

$$V_{ind} = 4.44 \cdot f \cdot N \cdot \Phi \tag{2.11}$$

where f is the frequency of the applied electromagnetic field, N is the number of turns, Φ is the maximum net flux that passes through coil. As the flux that passes through the coil is directly proportional to the area covered by coil, smaller diameter means decreased voltage. This equation also implies that as the frequency or number of turns increases, induced voltage will increase. For this system, frequency is chosen about 100 kHz.

At the primary side, ferrite core can be added to design to decrease the electromagnetic radiation and to increase the coupling [2]. For ferrite backing, EPCOS® PS35x10.8 with N22 material is chosen, which is suitable for 40 kHz to 400 kHz applications. It is a half core with 15.7mm inner diameter and 35mm outer diameter. More details of this product are given at appendix A.

Another criterion is that outer diameter of primary coil should be larger then outer diameter of secondary where inner diameter of primary winding should be smaller than inner diameter of receiver [8].

Winding resistance should be low. Using thick wires to decrease resistance causes skin effect, which dramatically increases AC resistance. In order to alleviate skin effect, diameter of the wires should satisfy the condition: $d \leq 2\delta$, where d is the diameter δ is the skin depth of at selected frequency [12]. At 100 kHz, skin depth for copper is calculated as $\delta = 0.209$ mm (Appendix B). Such a thin wire will increase the

resistance very much. Many wires of this thickness can be paralleled together to provide low resistances. These wire bundles are called litz wires. For windings of coils, litz wires will be used.

Based on these boundaries and chosen materials, Maxwell 3D® models are developed. Maxwell 3D®, is a finite element analysis (FEA) program which can calculate self and mutual inductances, and hence coefficient of coupling of 3D objects.

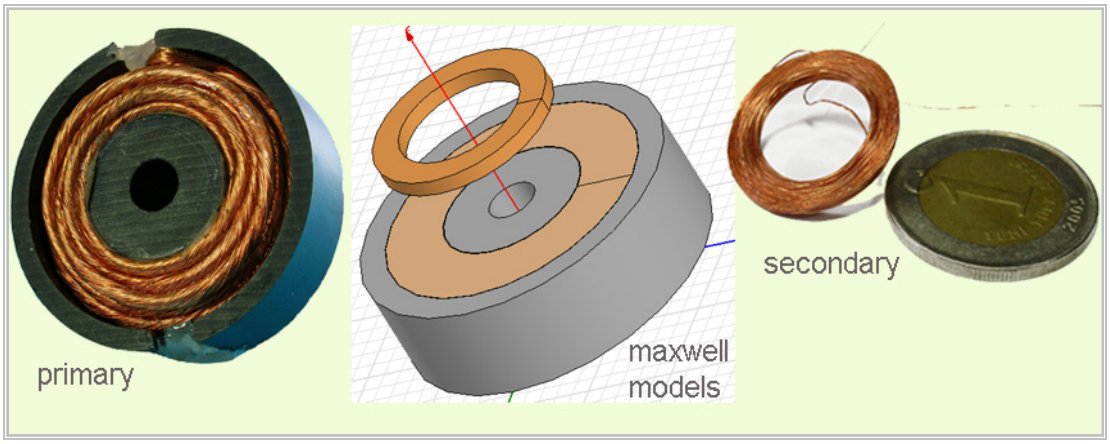

Figure 2.9: coils and Maxwell 3D® model

In following parts, variation of coupling coefficient will be traced as any change in distance between coils, alignment, winding window dimensions and diameter of the coil.

2.3.1. Winding Window width and height vs. coupling

While determining receiver coil dimensions, sizing cross section of the winding would be a good point to start. In order to observe the effects of winding window width (*w*) and height (*h*), coupling will be traced while keeping cross section area of winding constant. As depicted at Figure 2.10, window width is directly proportional to coupling. 3mm increase in width increased coupling from 0.15 to 0.19. However, at Figure 2.11, there is an inverse proportion between window height and coupling. Increasing height causes decrease in coupling, which is totally undesirable.

Based on these simulation results, a winding height and width are proposed as 1.5 mm and 4 mm, respectively. But, while constructing the coil, height deviated from the expected size. It was 1.75 mm. So, rest of the simulations are constructed for 1.75 mm x 4 mm coil.

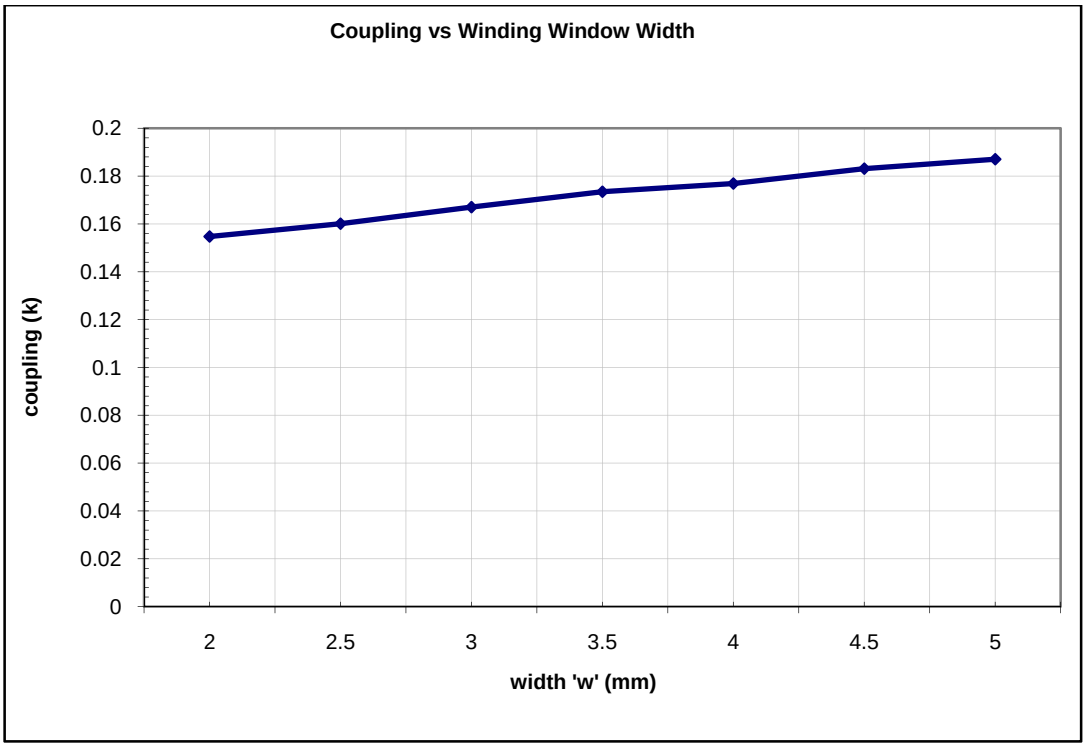

Figure 2.10: Coupling vs. Winding Window Width

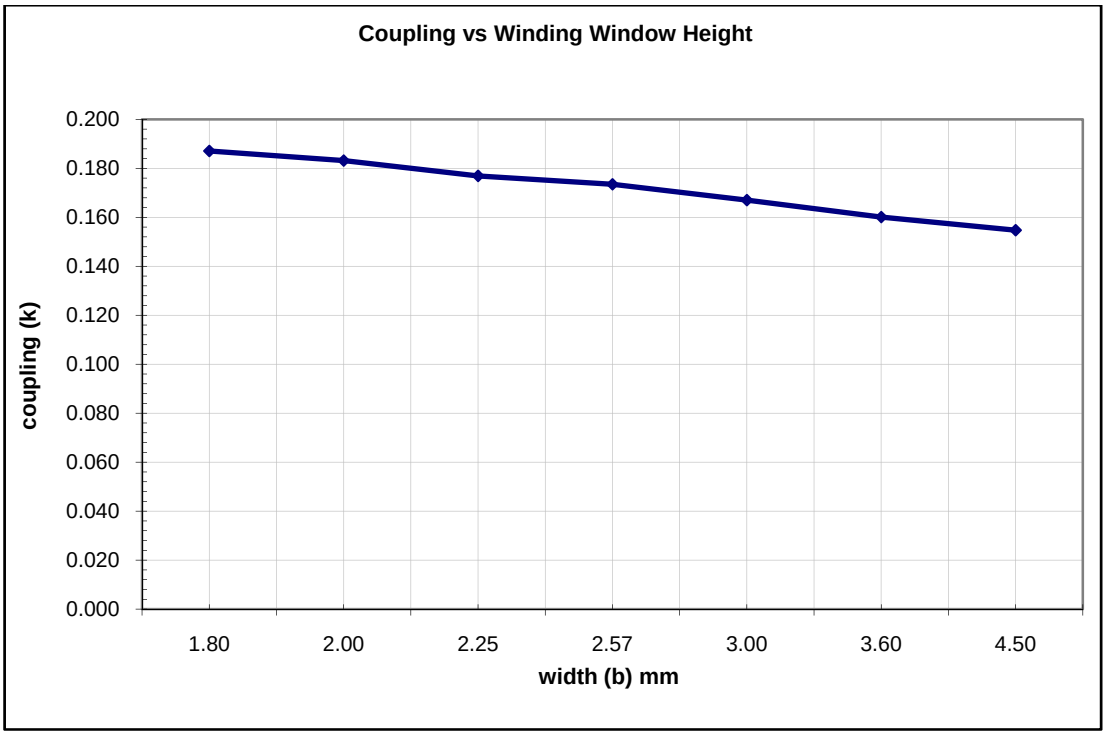

Figure 2.11: Winding Window height vs. coupling

2.3.2. Coil Diameter vs. Coupling

After setting winding window height and width, effect of coil diameter on coupling can be tracked. Also note that during simulation, coil separation is kept at 10mm. FEA simulation result is shown at Figure 2.12. Around 20mm, coil has an optimum diameter. Besides, there is not a significant variation in coupling between 18mm and 22mm. considering these results and equation (2.11) diameter is chosen as 24mm.

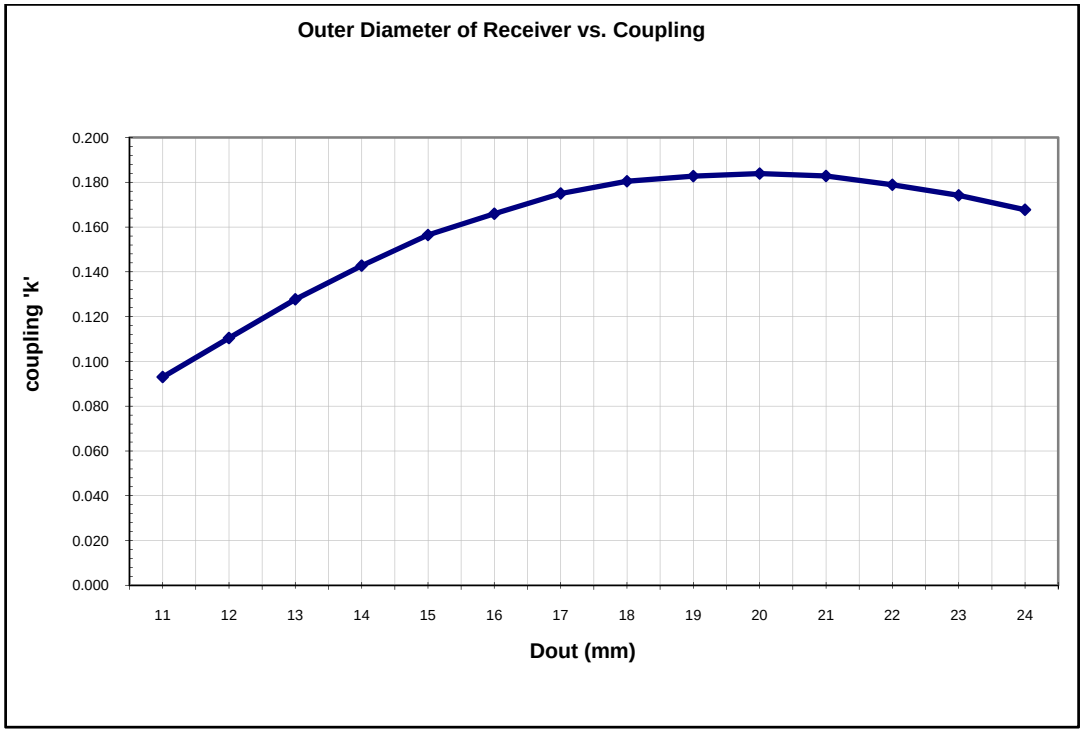

Figure 2.12: Outer Diameter vs. coupling

2.3.3. Horizontal misalignment vs. Coupling

Simulation result implies that coils are very immune to horizontal misalignment. At Figure 2.13, up to 2mm of misalignment does not affect coupling considerable. After 2mm, coupling degrades but it may be tolerated if a larger diameter coil is used.

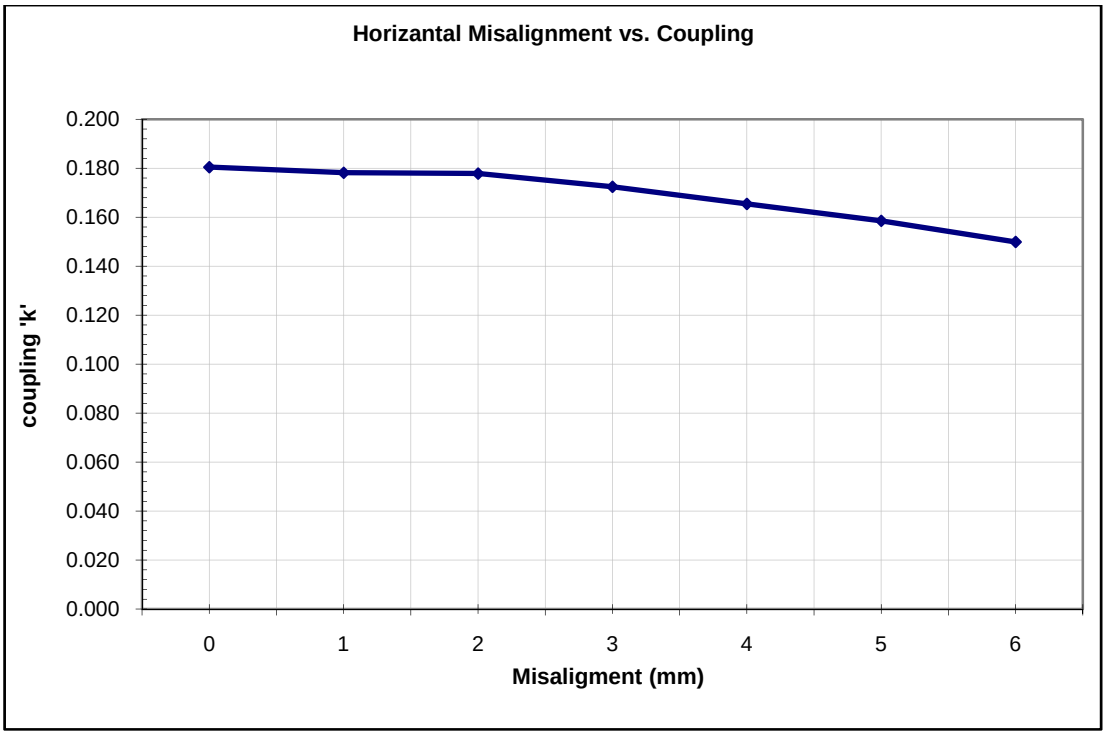

Figure 2.13: Horizontal misalignment vs. coupling

2.3.4. Angular misalignment vs. coupling

Figure 2.14 shows the effect of variation of angular misalignment on coupling. Normally system is not expected to deviated 45°, but simulation was run in a wide range. Apparently, deviation in angle notably effects coupling.

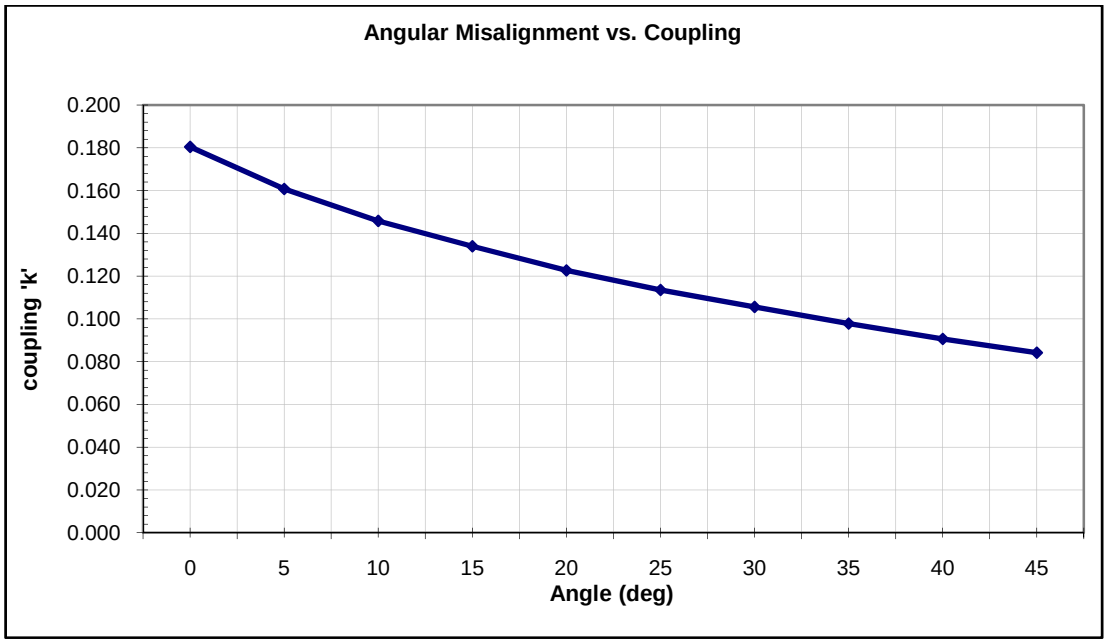

Figure 2.14: Angular Misalignment vs. coupling

2.3.5. Distance vs. Coupling

Separation between coils has a dominant effect on coefficient of coupling as expected. Other parameter variations have minor effects on coupling compared to effect of distance. From 5mm to 22mm, coupling varies from 0.4 to 0.35. In this thesis, working distance will be about 10mm. At that point, coefficient of coupling is about 0.16.

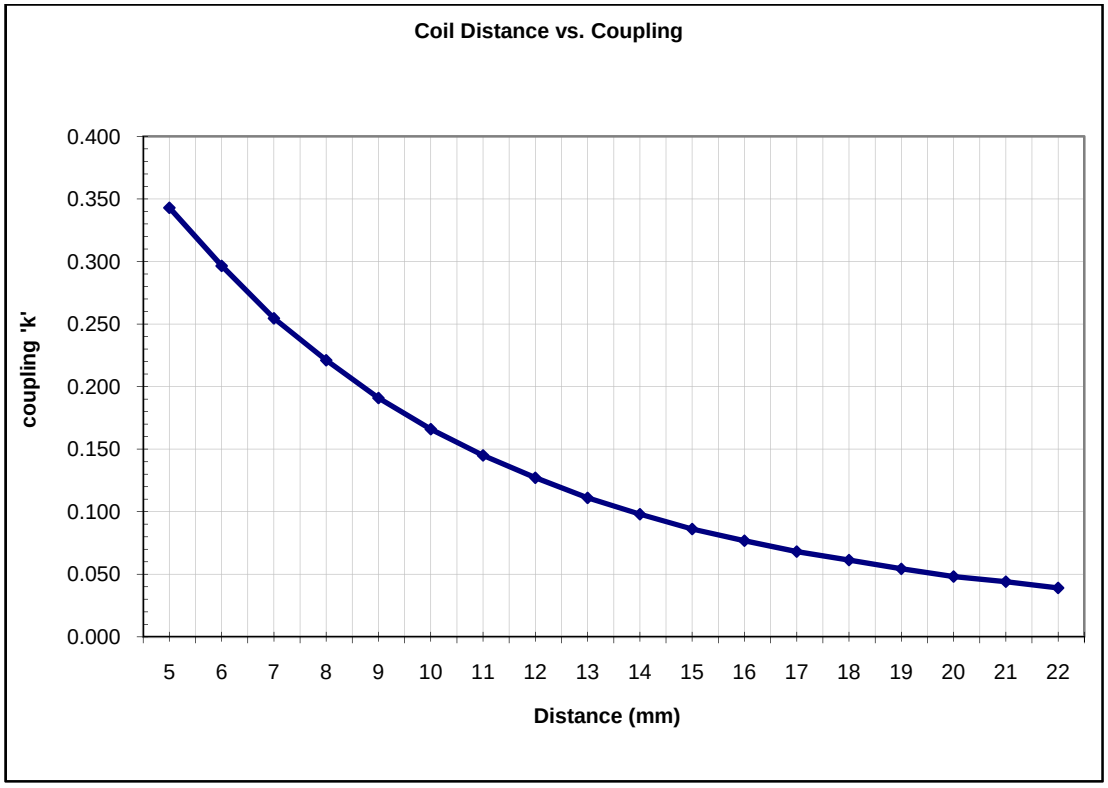

Figure 2.15: Coil distance vs. Coupling

2.3.6. Final Designs

In accordance with all simulation results, two final receiver designs are determined. Their properties are given at Table 2.1.

Table 2.1: Final coil design parameters

	Receiver Coil A	**Receiver Coil B**
Outer Dimater	25mm	23mm
Winding window height	1.75mm	1.75mm
Winding window width	4mm	4mm
Numer of strands	3	2
Number of turns	50	85

Also, primary coil is designed to fit the window area of ferrite core. It also has winding made of litz wire with 64 strands and 17 turns.

By employing Maxwell 3D®, inductances and coefficients of coupling are calculated for final designs at 10 mm distance. Maxwell simulation outputs are listed in Table 2.2.

Table 2.2: Maxwell 3D outputs for final coil designs

	Transmitter Coil	**Receiver Coil A**	**Receiver Coil B**
Inductance	24.2μH	82.8μH	211.3μH
Mutual inductance	-	7.8μH	11.9μH
Coef. of coupling	-	0.180	0.166

In order to validate simulation results, designed coils are measured with Agilent 6243 LCR meter equipment. Maxwell 3D has given quite successful results as seen at Table 2.3. Q is quality factors of coils, and formulated as,

$$Q = \frac{2\pi fL}{R} \tag{2.12}$$

Table 2.3: Measured results for coils

	Transmitter Coil	**Receiver Coil A**	**Receiver Coil B**
Inductance	23.1μH	83μH	200μH
Rac @ 100kHz	0.162 Ω	2.1Ω	3.3Ω
Q	88	35	38

2.4. Drive and Receiver Circuits

For driving primary coil, half bridge topology is chosen. All power components are chosen to have minimum resistance at working frequency. Switching MOSFETs are chosen IRLR3705Z, which has R_{DSon}=10mΩ. Voltage divider capacitors are ultra low equivalent series resistance (ESR) type capacitors. At the secondary side, 1N4148 diodes are used for rectification as they are suitable for high frequency applications. For circuit schematics please refer to appendix C and D. Two different power resistors are used to represent the load resistance. One of the resistors was 40Ω and the other is 200Ω. While tests are running for this set up, PSpice simulations are done. A similar circuit is realized in PSpice which is demonstrated at Figure 2.16.

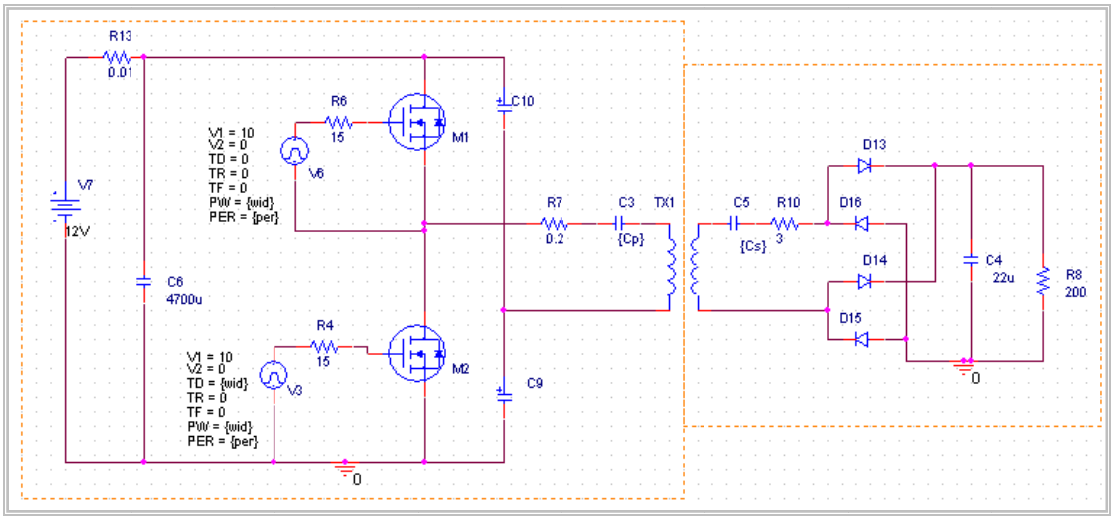

Figure 2.16: PSpice circuit

2.5. Comparing simulations and measurements

For validating accuracy of the PSpice model, a test set up is built with both Coil A and Coil B. Distance between coils is set to 10mm with a negligible horizontal misalignment. Calculated coefficient of couplings with Maxwell 3D are utilized at PSpice simulations. Resonance frequency is set approximately to 101 kHz.

Following tables and figures, clearly confirms that built PSpice model is quite accurate. Correlation between both simulations and measurements proves the consistency of the model.

Table 2.4 shows results and measurements at 200Ω load with Coil A. At 101 kHz, which is resonant frequency for both sides, induced voltage has maximum value. As the frequency deviates from resonance frequency, induced voltage degrades immediately. Maximum efficiency is reached at 101 kHz, too. As depicted at **Table 2.5** system has better efficiencies for the all frequencies compared to 200Ω load.

When receiver coil changed to Coil B, overall efficiencies are increased. Efficiency is reached up to 60%. Maximum induced voltage is at 100 kHz, slightly lower than resonant frequency, due to increased loading.

In both cases, power transfer ratio is reached the required levels. By varying frequency can be altered depending on the required power request.

Table 2.4: Measurements and Simulation results for Coil A at 200Ω load

	Secondary				**Primary**		
freq	**I (mA)**	**V (V)**	**V (PSpice)**	**P (W)**	**I (mA)**	**P (W)**	**Eff. (%)**
95k	46	9.2	10.6	0.42	254	2.54	16.7
96k	58	12	12.8	0.70	350	3.50	19.9
97k	75	15	16.2	1.13	540	5.40	20.8
98k	102	20.77	21.3	2.12	943	9.43	22.5
99k	151	30.6	28.7	4.62	1917	19.17	24.1
100k	230	46	40.5	10.58	4250	42.50	24.9
101k	247	50	52	12.35	4870	48.70	25.4
102k	173	34.8	47	6.02	2500	25.00	24.1
103k	119	24	35.2	2.86	1270	12.70	22.5
104k	88	17.83	26.1	1.57	742	7.42	21.1
105k	69	14	19.5	0.97	498	4.98	19.4

Table 2.5: Measurements and Simulation results for Coil A at 40Ω load

	Secondary				Primary		
freq	**I (mA)**	**V (V)**	**V (PSpice)**	**P (W)**	**I (mA)**	**P (W)**	**Eff. (%)**
95k	192	7.96	8.5	1.53	413	4.13	37.0
96k	242	10	10.2	2.42	593	5.93	40.8
97k	310	12.89	12.3	4.00	911	9.11	43.9
98k	405	16.8	15	6.80	1451	14.51	46.9
99k	517	21.4	17.6	11.06	2266	22.66	48.8
100k	587	24.26	20.2	14.24	2838	28.38	50.2
101k	567	23.4	21.5	13.27	2637	26.37	50.3
102k	479	19.83	20.9	9.50	1950	19.5	48.7
103k	390	16.1	19.1	6.28	1335	13.35	47.0
104k	320	13.17	16	4.21	932	9.32	45.2
105k	267	11	14.2	2.94	689	6.89	42.6

Table 2.6: Measurements and Simulation results for Coil B at 200Ω load

	Secondary				Primary		
freq	**I (mA)**	**V (V)**	**V (PSpice)**	**P (W)**	**I (mA)**	**P (W)**	**Eff. (%)**
95k	72	14.58	14.7	1.05	329	3.29	31.9
96k	89	18	17.9	1.60	477	4.77	33.6
97k	114	23	21.6	2.62	720	7.20	36.4
98k	152	30.5	27.5	4.64	1200	12.00	38.6
99k	209	41.8	32	8.74	2120	21.20	41.2
100k	272	54.2	45	14.74	3500	35	42.1
101k	277	55.3	55	15.32	3580	35.80	42.8
102k	220	44.2	53.7	9.72	2330	23.3	41.7
103k	167	33.5	44	5.59	1383	13.83	40.5
104k	131	26.15	35	3.43	883	8.83	38.8
105k	106	21.22	28	2.25	604	6.04	37.2

Table 2.7: Measurements and Simulation results for Coil B at 40Ω load

	Secondary				Primary		
freq	**I (mA)**	**V (V)**	**V (PSpice)**	**P (W)**	**I (mA)**	**P (W)**	**Eff. (%)**
95k	300	12.32	12.2	3.70	700	7	52.8
96k	351	14.43	14.1	5.06	932	9.32	54.3
97k	400	16.43	15.8	6.57	1165	11.65	56.4
98k	439	18.04	17.2	7.92	1356	13.56	58.4
99k	463	19	17.7	8.80	1483	14.83	59.3
100k	466	19.13	18.4	8.91	1483	14.83	60.1
101k	460	18.88	18.3	8.68	1440	14.4	60.3
102k	441	18.13	17.6	8.00	1335	13.35	59.9
103k	417	17.11	17	7.13	1208	12.08	59.1
104k	387	15.9	16	6.15	1060	10.6	58.1
105k	356	14.64	15.2	5.21	922	9.22	56.5

In order to evaluate the performance of PSpice, following figures can be referred. PSpice simulations correlate measurements in most cases. However, at some frequencies there are more deviations then others. The reason is that inductance values may vary slightly in practice. In addition, used resonance capacitors have a tolerance of 10%, which causes de-tuning of resonant frequency. As resonant tanks are very sensitive to frequency deviations, difference between measured results is quite normal.

In addition, during measurements temperature of primary coil may change depending on the current that pass through the winding. Temperature affects the inductance value and causes deviation the resonant obviously. In PSpice temperature is kept constant during simulation.

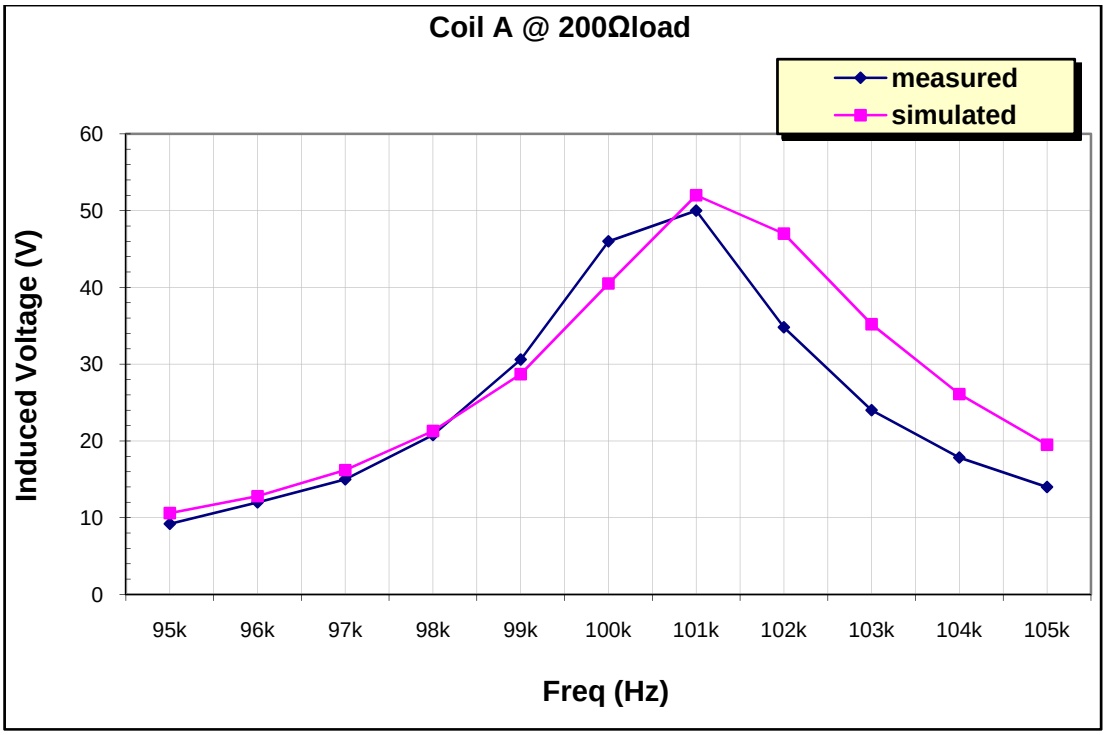

Figure 2.17: Measured and simulated results for Coil A @ 200Ω load

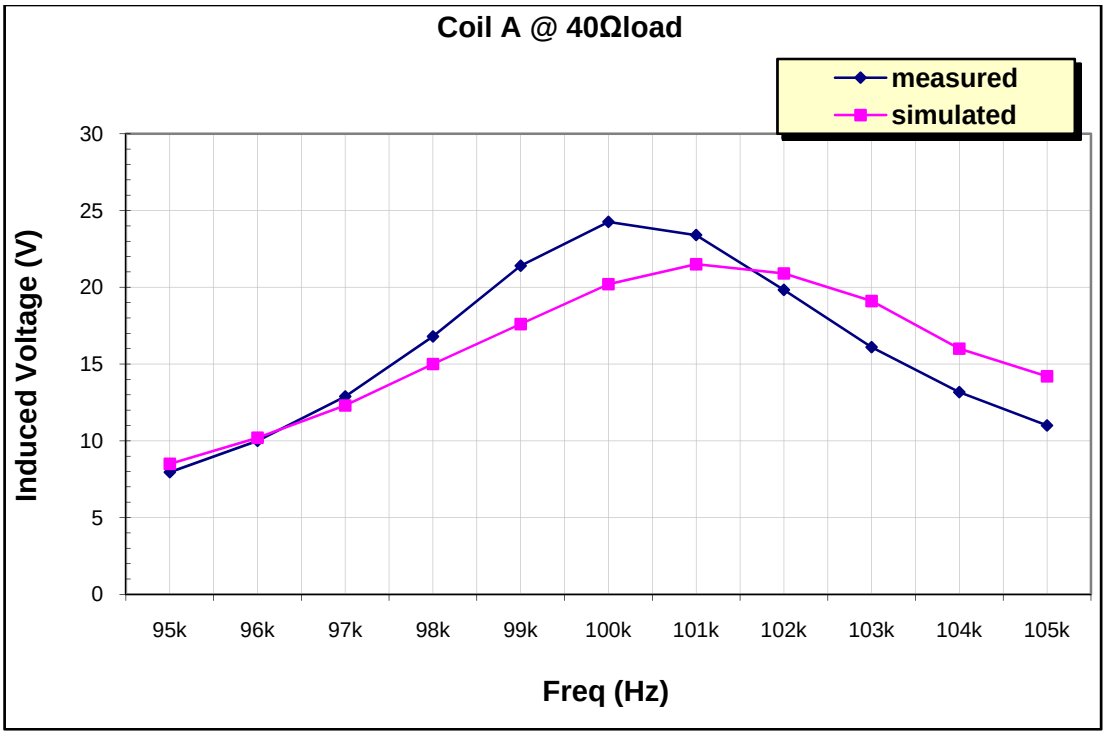

Figure 2.18: Measured and simulated results for Coil A @ 40Ω load

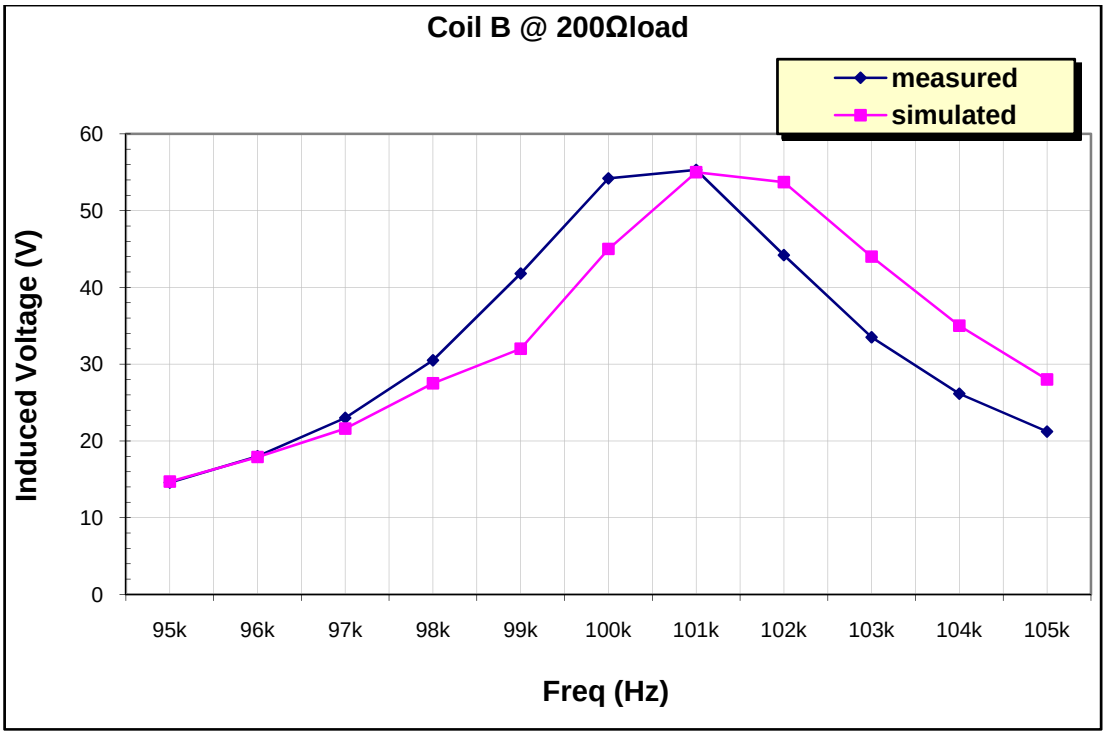

Figure 2.19: Measured and simulated results for Coil B @ 200Ω load

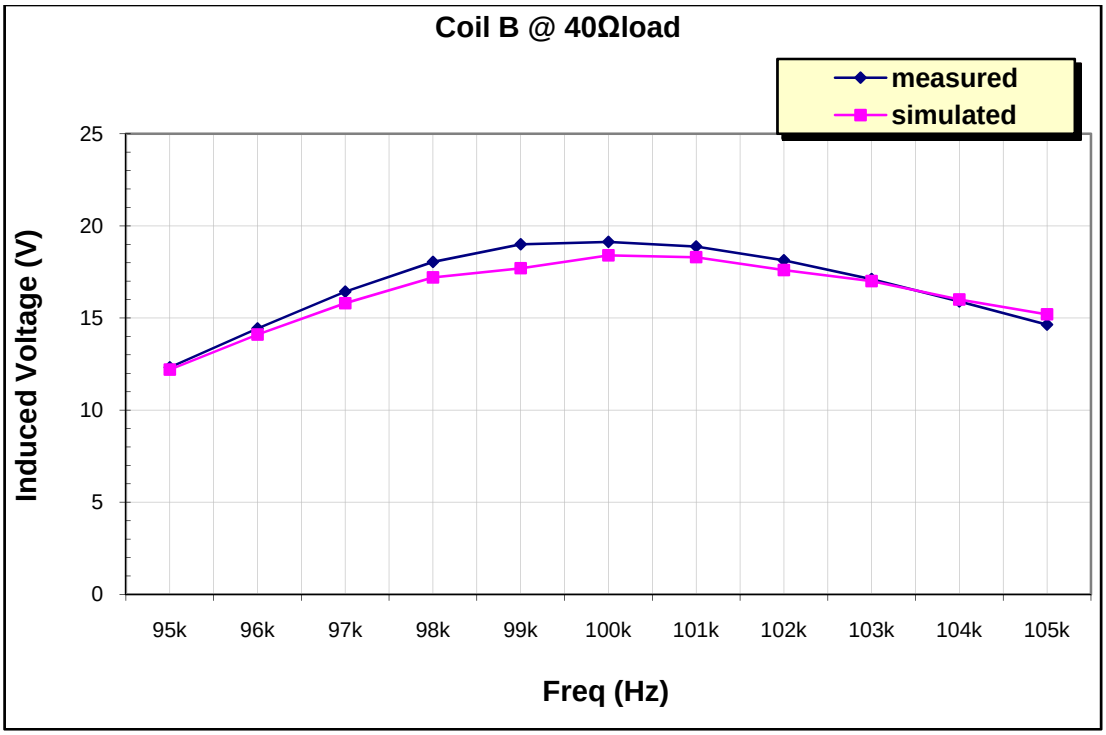

Figure 2.20: Measured and simulated results for Coil B @ 40Ω load

3. WIRELESS TRANSFER OF INFORMATION

Transferring information is another important issue in this thesis. Data transfer can be unidirectional or bidirectional. In this application data transfer will be bidirectional. Transmitted data will include motor direction, motor rotation and additional data if required. Received data includes confirmation data.

Generally, there are two ways of data communication; one of them is using additional coils with a few turns on both primary and secondary sides [12]. They are driven with an independent source at higher frequency then the resonant frequency in order to prevent any interference with power driver system [14]. Main drawback of this method is that it requires additional coils and cable to be connected to primary and secondary coils. In these systems, information is sent to primary coil again by using the same additional coils.

Another way of data communication is to use receiver and transmitter coils for both power and information transfer. There are different methods that inject information into power signal. One of them utilizes amplitude shift keying (ASK). At this method, amplitude of induced voltage at secondary side is altered by changing the transmitter voltage. At the secondary side, amplitude of the induced voltage is tracked by microcontrollers after they are filtered and reshaped [1]. A further way in ASK method is turning on and turning off the transmitter for a very short periods. Amplitude of the induced voltage at the secondary side switches between zero and non zero voltages [15].

When the subject is transferring data from secondary to primary, the common method is changing the load at secondary. When the load at secondary side is changes, the current in the primary side is also affected proportionally. A current sensor at the primary side tracks any change at the current. So a microcontroller at the primary side can decode information, injected in current.

3.1. Sending Data to Secondary

While sending data from primary to secondary, two methods were proposed at the beginning of this thesis. The first one was ON-OFF keying (OOK). In this method, carrier signal turned on/off for logic 0 / logic 1. So the absence or existence of carriers signal indicates the logic level. This method was used at the beginning of thesis, and was successful to transmit data. However, the carrier signal also the power transmitting signal. So absence of carrier signal, also, means no power will be delivered to secondary part. As the energy cut-off occurs for only small intervals, (e.g. ~400usec for each bit), the secondary circuit can use energy stored at the capacitors. The disadvantage of this method is that system requires more power when motor runs, and capacitors would not be enough to recover energy during energy cut-offs. So this method is dismissed.

The second method for transmitting data is amplitude shift keying (ASK). In this method carrier signal is never turned off. But the amplitude of carrier signal is altered. Interval times between two different amplitudes indicate logic data. Continuity of carrier signal means continuity of power transmission.

ASK is one of the common methods in these systems. All the systems use a basic circuitry that changes the input voltage of DC/AC inverter. A resistor connected series to power input of inverter. A power MOSFET which has a very low drain to source resistance is connected parallel to resistor. Resistor has a small value (about 1 Ω), but causes a certain voltage drop depending on the current flowing to the inverter. As MOSFET across the resistor has a very low ON resistance, most of the current flows though the MOSFET when it is turned on. When the transistor is turned on voltage drop will be significantly lower compared the voltage drop across the resistor when transistor is off. By turning on/off MOSFET across the resistor, amplitude of signal at the output of resonant converter is altered. Turn on and off times of the MOSFET indicates the logic level. However, these sorts of systems require additional circuitry for sending data.

In this thesis, a new method, which utilizes a software based method, is proposed for amplitude shifting. The new method takes the advantage of sensitivity of resonant converters to frequency changes. As mentioned previously, gain of a resonant converter is a function of frequency. Variation at the frequency of driving signal of

resonant tank causes variation at the voltage across the primary inductor. As a result, any amplitude change at primary voltage will be reflected to the secondary side. A data filtering circuitry retrieves data and sends to microcontroller. Figure 3.1 shows the general data transfer scheme.

Carrier signal basically has two amplitudes during transmission. Duration of the low amplitude signal indicates the logic level. For example 250µs duration means logic 1, while 500µs duration means logic 0. At Figure 3.2, 'induced voltage at secondary side' shows a sample logic data transfer. In order to retrieve the data from carrier signal a data filtering circuitry is used. At the filtered signal (Figure 3.2), the interval time between a falling edge and a rising edge designates the logic data. In the same manner, the interval between two falling (or rising) edge can also be used to recover logic data. The microcontroller utilizes a timing algorithm which tracks the intervals to get data.

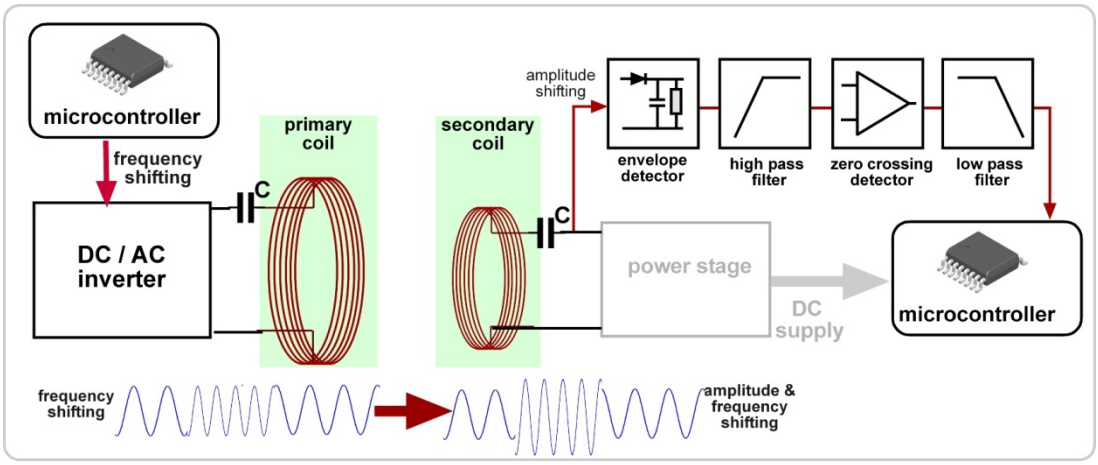

Figure 3.1: Data transfer scheme from to Primary to Secondary

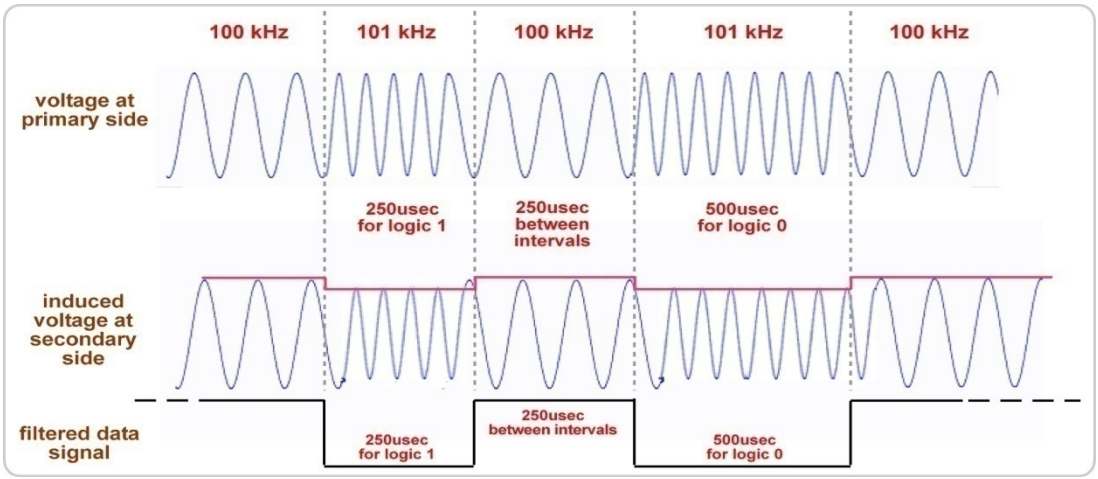

Figure 3.2: Signal shapes while sending data to secondary

Data filtering system consists of four basic data retrieving elements. As depicted at Figure 3.1, data signal passes through envelope detector, high pass filter, zero crossing detector and low pass, respectively. This is the most basic data filtering scheme and requires a few components to realize. Considering that there is a few space in secondary part, it is advantageous to use less components. In this system, envelope detector tracks the amplitude of carrier signal. Output signal at the envelope detector has DC signal in it. In order to eliminate DC component, a high pass filter is used. High pass filter is followed by zero crossing detector, which is an operational amplifier (OPAMP) working as a comparator. At this point analogue signal is digitalized. A low pass filter eliminates any high frequency noise added at OPAMP. Output signals during data recovery process are shown at Figure 3.3 step by step.

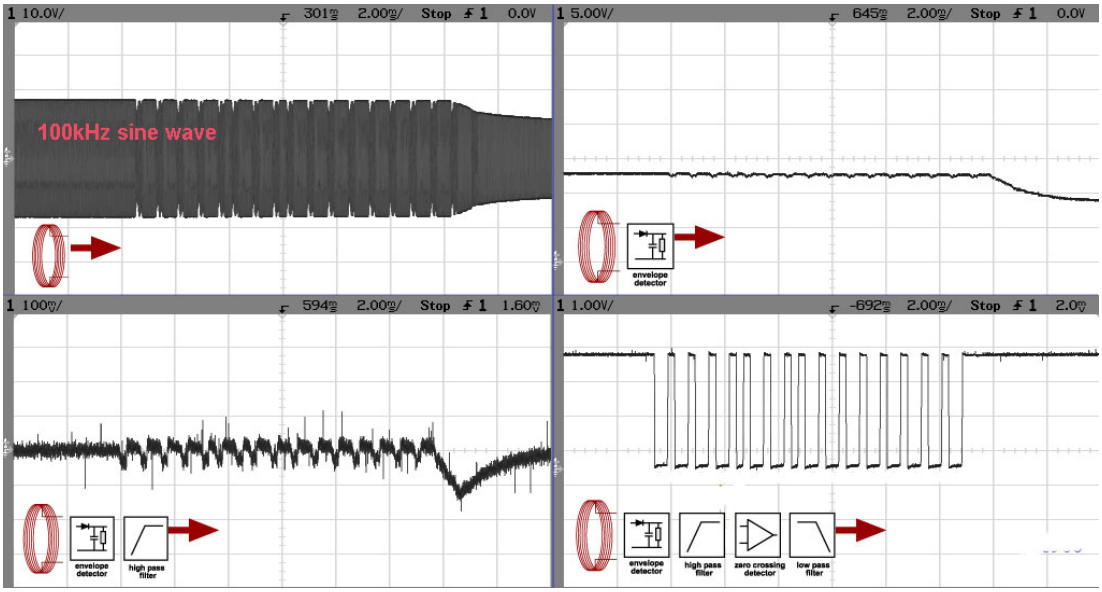

Figure 3.3: Data signal processing steps (sending from primary to secondary)

At Figure 3.4, final output signal is zoomed and a sample data signal is decoded as an example. Long intervals point to logic 0. Short intervals point to logic 1, as well. Decoded signal at the figure is ‘0900’ in hex notation. Generally, communication scheme is similar to the asynchronous serial communication, such as RS232. Microcontroller starts reading data when a falling edge is sensed at the input. Different from asynchronous scheme, microcontroller gets data by measuring the intervals between falling and rising edges.

Transfer rate of the system is about 1.6 bits/second. As the system is intended to transfer very limited data, transfer rate is fair enough.

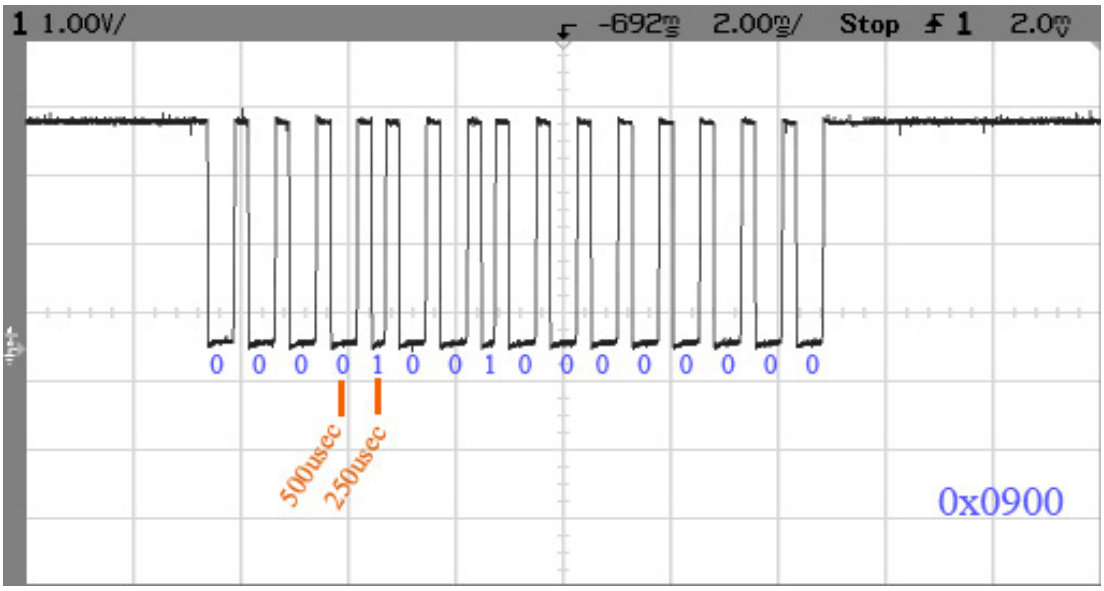

Figure 3.4: Recovered data, at the microcontroller input (sending)

3.2. Receiving Data from secondary

Receiving data from secondary, in other words sending data to primary is achieved by changing the load at the secondary. Similar method is also used in contactless ID cards. Also at [1], data transfer is realized with a similar method, but secondary side resonant topology is different.

Variation at the load changes current and voltage at the primary resonant tank. As the load at the secondary side increases, the current at the primary side will increase. And the voltage across the primary inductor (and capacitor, as well) will decrease due to internal resistances. It is possible to trace either current fluctuations or voltage fluctuations to recover received data. In the thesis, voltage will be traced for receiving data.

At Figure 3.5, general data transfer scheme for sending data to primary is shown. In order to change load at the secondary side, a MOSFET is introduced to system. Actually, there is not any extra load resistance in the system. If the MOSFET is turned on, all the current flows through it. As the MOSFET has a drain to source resistance of ~1 Ω, the load seen by primary side is very high. At Figure 3.6, resulting signal shapes are demonstrated depending on MOSFET on/off states.

Voltage variation is traced at the connection node of capacitor and inductor coil at resonant tank. Data filtering and recovery technique is quite analogous to previous

one (sending data to secondary). Figure 3.7 demonstrates the signals during data recovery process.

Received data scheme is same as the scheme used for sending data to secondary. As seen at Figure 3.6, filtered data signal is normally logic 1. When the MOSFET turned on, recovered signal drops to logic 0. Data interval times are same as previous. In the same manner, microcontroller at the primary side decodes data according to durations of signal. A sample received data is shown at Figure 3.8.

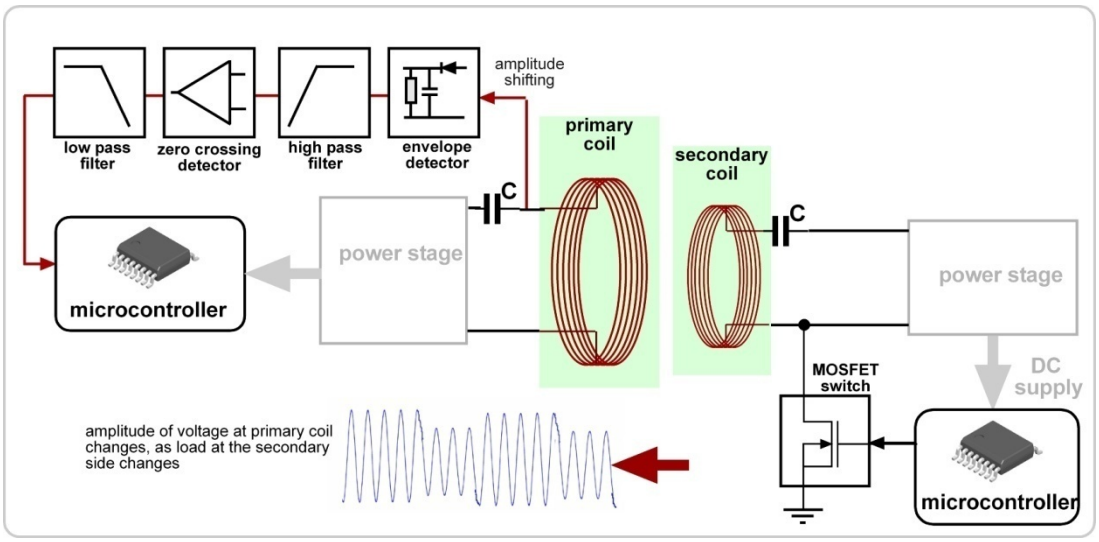

Figure 3.5: Data transfer scheme from to Secondary to Primary

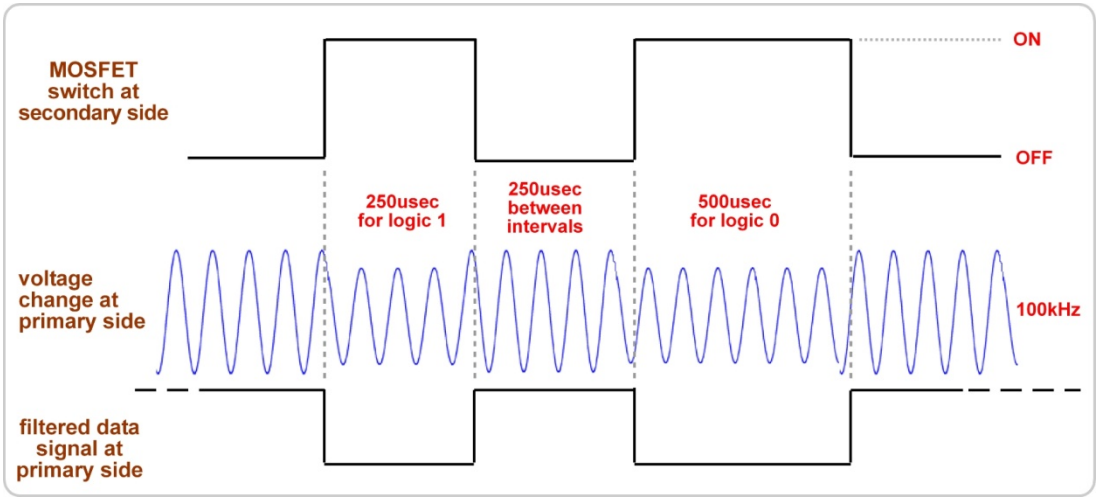

Figure 3.6: Signal shapes while sending data to primary

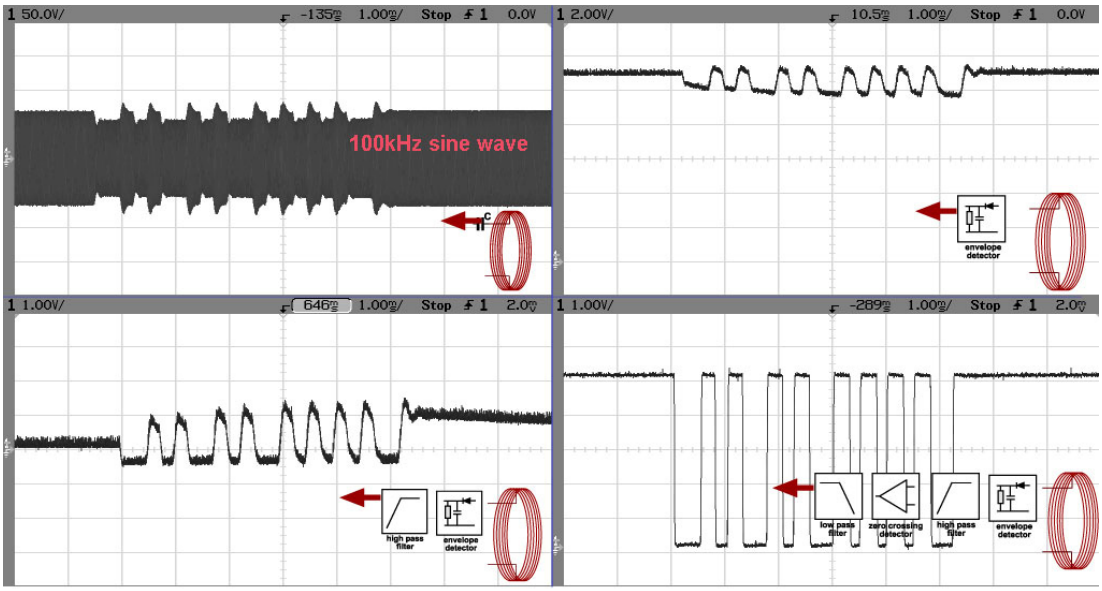

Figure 3.7: Data signal processing steps (sending from secondary to primary)

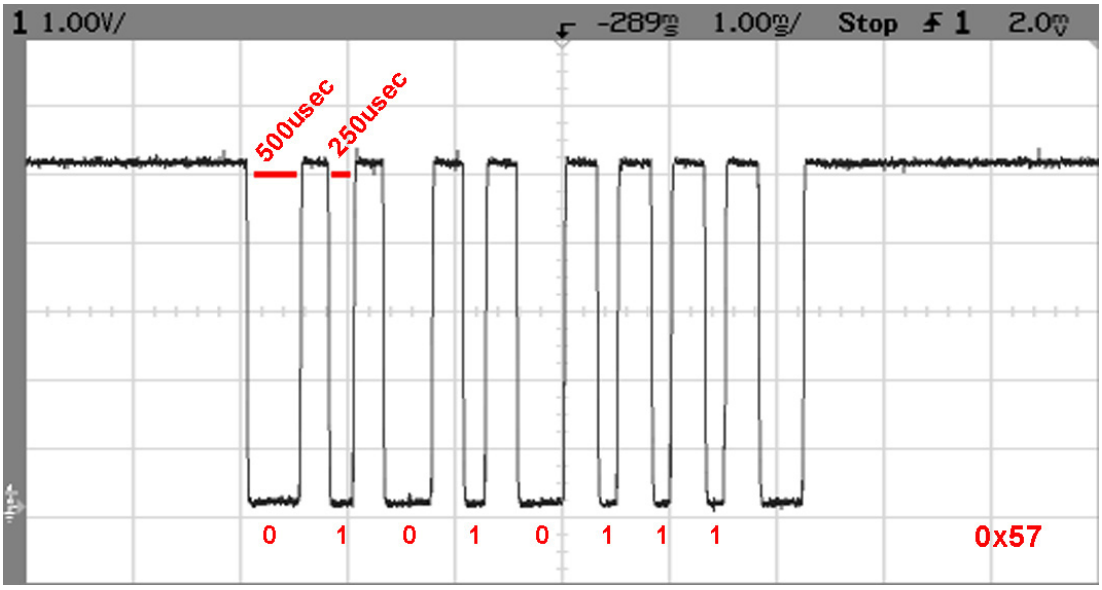

Figure 3.8: Recovered data, at the microcontroller input (receiving)

3.3. Communication between primary and secondary

As mentioned previously, the communication system is half duplex. Data transfer can be at one direction at a time. If both primary and secondary sides try to send data at the same time, a confliction will occur. Received data on both sides will be corrupted. On the other side, it is not required to send or receive data at the same time. Only a few amounts of information are enough to control the system.

A data transfer protocol is developed in order to provide a stable data communication between sides. According to protocol, the primary side never sends data unless secondary side sends a confirmation data. After secondary sends confirmation data, it switches to listening status and waits for motor control data. At the same time, when confirmation data received at the primary side, primary sends motor control data. Then motor runs according to received data. When motor stops, secondary sends a data which confirms that motor is stopped. At Figure 3.9, data and energy flow is explained step by step.

The data which is sent to secondary is two byte data and includes rotational direction of motor, number of turns. The received data from secondary is a one byte data, which has different values for confirmation and motor stop situations. If primary cannot get any of these codes, it does not send any data to secondary for safety reasons. If primary gets no confirmation in certain time, it does not send a data to secondary, as well.

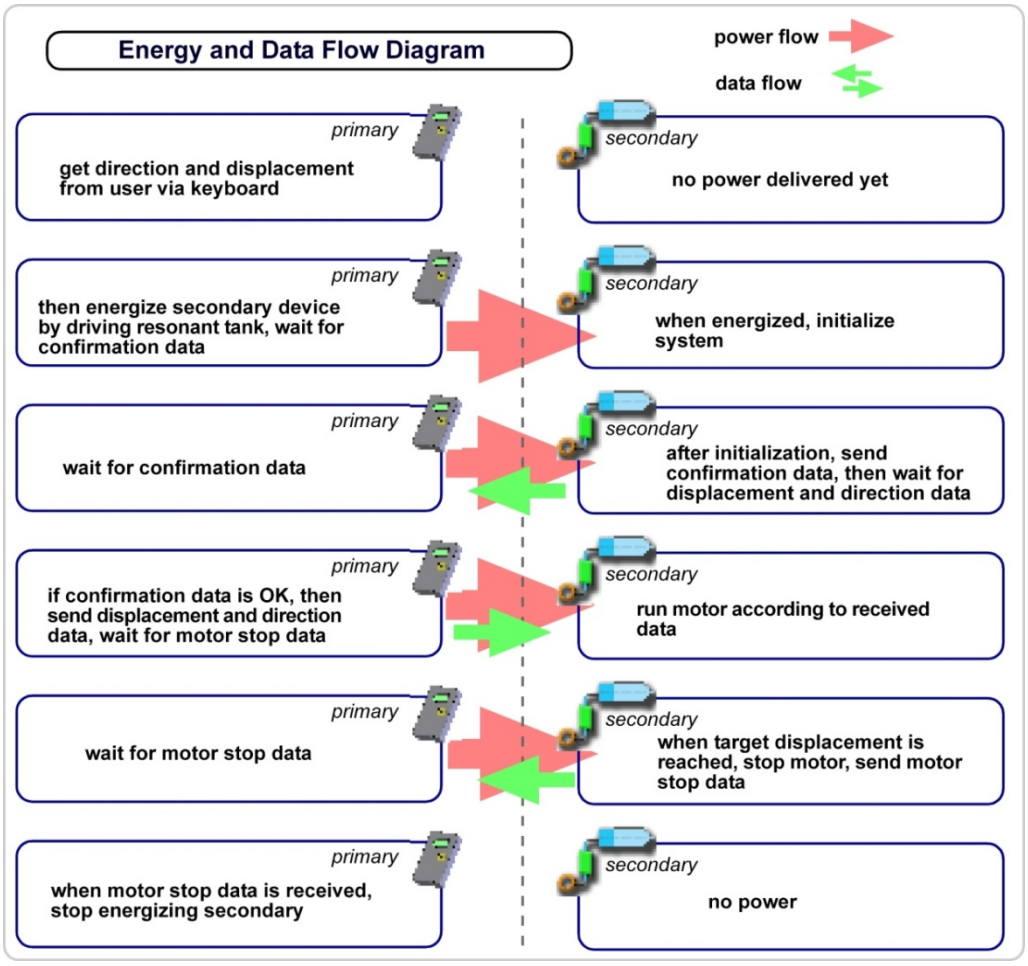

Figure 3.9: Energy and Data flow diagram

4. MOTOR DRIVE and LINEAR POSITIONING

Mechanical system is aimed to convert rotational motion into a linear motion. Most important feature of the system is that it allows sensitive positioning. The system consists of a DC motor, followed by a planetary gear box and lead screw mechanism. Also, an encoder is mounted on the motor for feedback. Motor is driven with a special motor driver chip, which is capable of bi-directional motor drive. Encoder output is fed to microcontroller for feedback. As mentioned previously, microcontroller meant to run motor until requested number of turns is reached. General system topology is depicted at Figure 4.1.

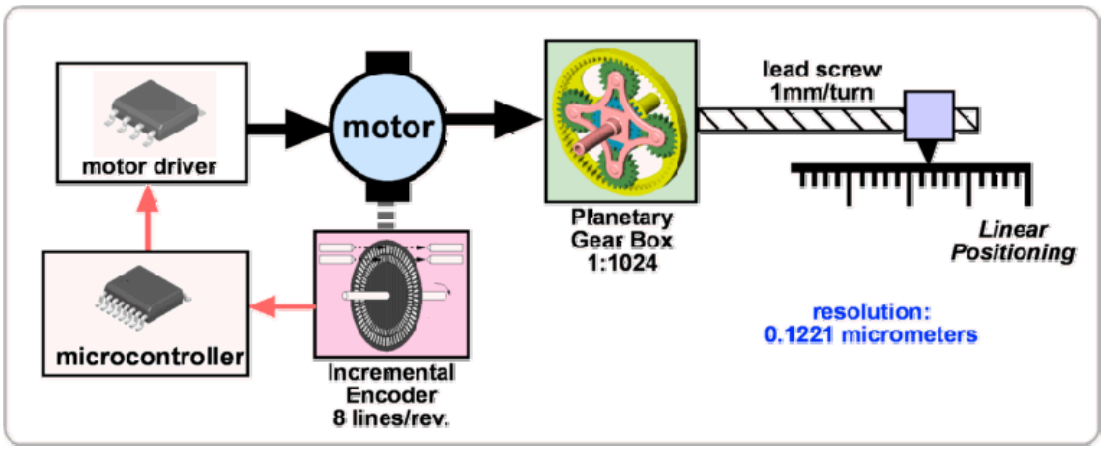

Figure 4.1: Motor Control and Mechanical Topology

DC motor is a 1.3 W Faulhaber Series 1224 012S micro motor. Its nominal speed is 12000 rpm and it has a nominal torque of 1mNm [16]. In order to achieve a sensitive positioning, a high ratio planetary gear box is implemented right after the motor. Planetary gear is also a Faulhaber product, which comply with 1224 012S micro motors. Chosen gear ratio is 1:1024, which considerably decreases rotational speed. At a ratio of 1:1024, gear efficiency is 55%, and capable of providing a torque of 300 mNm at the output [17]. Planetary gear is followed by a lead screw mechanism, which converts rotational motion to translational motion. The advantage of lead screw mechanism is that it prevents linear motion in absence of rotational motion. Even if motor is removed from system, linear position will tend to stand still.

Male and female threads are designed according to ISO metric M10x1 screw thread. Each turn of screw results in 1mm linear displacement. At this point, linear displacement can be calculated in terms of rotational motion. If 1 mm displacement achieved by 1024 turns of motor, then each turn of motor will result in,

$$\frac{1mm}{1024turns} \cong 0.9766\mu m / turn \tag{4.1}$$

In addition, motors provided with incremental encoders mounted on them. Encoder has two digital outputs with a resolution of 8 lines per revolution [18]. So the resolution of the is calculated as,

$$\frac{0.9766\mu m / turn}{8lines / turn} = 0.1221\mu m / line \tag{4.2}$$

The whole mechanical system is designed by Solid Works CAD drawing program. Parts are manufactured at Yeniyurt Gear and Machinery Co. Ltd. At Figure 4.2, CAD drawing and the mechanic system is shown.

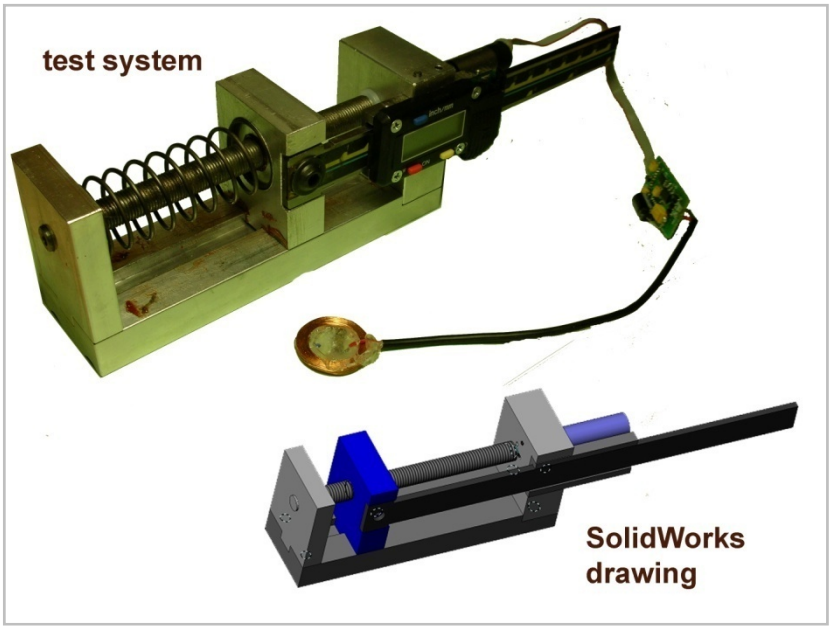

Figure 4.2: Solid Works drawing and realized system

The mechanical system is simulated with Matlab/SIMULINK including DC motor model. Simulations have revealed that motor speed can decrease to about 9000 rpm under full load. So, linear speed can change depending on the external load. But encoder will provide position data for accurate positioning. However, system components have backlashes. Such as, planetary gear has a backlash of 3º at no load.

In addition, lead screw mechanism has more backlash due to manufacturing limits. In order to suppress the backlash problem of lead screw, a spring is added to system, which works as preload.

When establishing the test rig, a measurement device is added to system. So, it will be possible to control if system works as expected. On the other hand, measuring device has only a resolution of 100 µm. Despite it will not possible to measure exact displacement, 100 µm is fair enough to observe system behaviour.

5. CONCLUSION

In this thesis, the aim was to design a system that is capable of driving a motorized linear positioning actuator by means of wireless power and information transfer. System gets displacement and direction of motor from end-user by using a keyboard and LCD interface. Primary system sends power information to secondary system to drive the motor in requested direction and amount.

For energy transfer part, coils and power drive systems are designed by employing Maxwell 3D and PSpice simulation tools. It has been shown that measurement on the test circuits are quite in compliance with the simulation results. Power transfer was successful up to 15mm, which is more than required. Power transfer efficiency has reached up to 60%. It is quite satisfying when separation of the coils considered.

For data transfer, a half duplex communication system is designed. A new method for transmitting data to secondary is proposed and realized. The new method eliminates hardware requirements by employing a software based technique. The new technique is proved to work stable on the test circuits. For transmitting data to primary, a voltage tracing method is used. For data transfer an ASK based modulation scheme is used. For encoding and decoding data a pulse width based method is proposed and realized. Data transfer rates are reached to ~1.6 kbits/s.

A linear positioning system is designed by using Solid Works. Mechanical system converts rotational motion to linear motion by means of lead screw mechanism. In order to increase mechanical resolution, a planetary gear box added between motor and lead screw. Planetary gear, also, increased output torque. Achieved liner mechanical resolution is about 0.1221 μm.

As a conclusion, proposed methods and simulations have shown to be valid on the realized electronic and mechanical systems. There is a considerably correlation between simulations and measurements. Constructed systems work as they are meant to be.

REFERENCES

[1] **Catrysse, M., Hermans, B. and Puers, R.**, 2004. An inductive power system with integrated bi-directional data-transmission, *Elsevier Sensors and Actuators A: Physical, Volume 115, **2-3**, 221-229*

[2] **Zierhofer, C.M. and Hochmair, E.S.**, 1996. Geometric Approach for Coupling Enhancement of Magnetically Coupled Coils, *IEEE Transactions on Biomedical Engineering, Vol. **43**, No. 7*

[3] **Nishimura, T.H., Eguchi, T., Hirachi, K., Maejima, Y., Kuwana, K., Saito, M.,** 1994. A Large Air Gap Flat Transformer for A Transcutaneous Energy Transmission System, *IEEE Power Electronics Specialists Conference,* June 1994, p.1323 - 1329 vol.2

[4] **Shiba, K., Tatsumi, E., Taenaka, Y. and Takano, H., 2002.** Analysis of specific absorption rate in biological tissue surrounding transcutaneous transformer for an artificial heart, *Japanese Society for Artificial Organs,* **5**, p.91-96

[5] **Fernández, C., Garcia, O., Prieto, R., Cobos, J.A., Gabriels, S. and Van Der Borght, G.,** 2002. Design Issues of a Coreless Transformer for a Contact-less Application, IEEE

[6] **Prof. Dr. Mehmet Kocaoğlu**, 2006, Personal contact

[7] **Pedder, D. A. G., Brown, A.D. and Skinner, J.A.,** 1999. A Contactless Electrical Energy Transmission System, *IEEE Transactions on Industrial Electronics, Vol. **46,** No. 1*

[8] **Ghahary, A. and Cho, B. H**., 1990, Design of Transcutaneous Energy Transmission System Using A Series Resonant Converter, *IEEE Transactions on Power Electronics, Vol. **7**, Issue 2, p.:261 - 269*

[9] **Nilsson, J. W. and Riedel, S.A.**, 2001. Electric Circuits, 6th ed., Prentice Hall, New Jersey

[10] **Jang, Y. and Jovanovic, M. M.**, 2003. A Contactless Electrical Energy Transmission System for Portable-Telephone Battery Chargers, *IEEE Transactions on Industrial Electronics, Vol. **50**, No. 3*

[11] **Rashid, M. H.**, 2004. Power Electronics, *3rd Ed., Pearson Education, India*

[12] **Mohan N., Undeland, T. M. and Robbins, W. P**., Power electronics, *2nd Ed., John Willy and Sons Publishing*

[13] **Joung, G. B. and Cho, B.H.,** 1998. An Energy Transmission System for an Artificial Heart Using Leakage Inductance Compensation of Transcutaneous Transformer, *IEEE Transactions on Power Electronics, Vol. **13**, No.6, p.1013-1019*

[14] **Bieler, T., Perrottet, M., Nguyen, V., Perriard, Y.,** 2002. Contactless Power an Information Transmission, *IEEE Tranasactıons on Industry Applications, Vol. 38,no. 5, p.1266-1272*

[15] **Kawamura, A., Ishioka, K. and Hirai, J.,** 1996. Wireless Transmission of Power and Information Through One High-Frequency Resonant AC Link Inverter Robot Manipulator Applications, *IEEE Transactions on Industry Applications, vol. **32**, No. 3*

[16] **Faulhaber Series 1224…S** DC Micro motors, datasheet, 'www.faulhaber.com'

[17] **Faulhaber Series 12/4** Planetary Gear heads, datasheet, 'www.faulhaber.com'

[18] **Faulhaber Series 05AB** Encoders, datasheet, 'www.faulhaber.com'

APPENDIX-A EPCOS FERRITE CORE

When realizing the transmitter coil, Epcos B65947 series PS35x10.8 core is used. Ferrite material was N22, which is suitable for 40 to 400 kHz applications. In order to simulate N22 with Maxwell 3D, B-H curve data is extracted from datasheet. Related B-H curve for N22 is shown at Figure A.1[1]

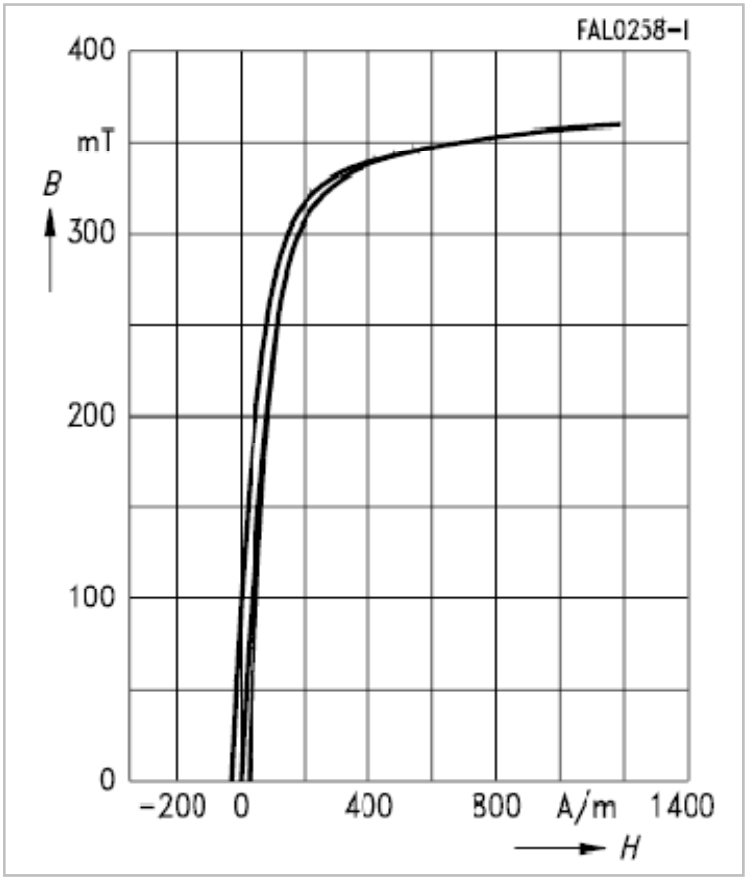

Figure A.1: B-H curve for N22 ferrite

.

[1] The graph at Figure A.1 is extracted from EPCOS datasheet for N22 materials

APPENDIX-B SKIN EFFECT

Skin depth, is the distance through which the amplitude of a travelling plane wave decreases by a factor e^{-1}. When an AC current passes through a conductor, it tends to move to the surface of the conductor. As a result, centre of the conductor does not carry any electrons. Thus, resistance of the conductor increases by frequency. This phenomenon is called skin effect. If the conductor diameter is chosen less then two times of skin depth then skin effect can be neglected. Skin depth is calculated by the following equation,

$$\delta = \frac{1}{\sqrt{\pi f \mu \sigma}} \quad \text{(meter)} \tag{B.1}$$

In this equation, *f* is the frequency; μ is permeability of copper and σ is conductivity of copper. For copper, $\mu = 4\pi \cdot 10^{-7} (H/m)$ and $\sigma = 5.80 \cdot 10^{7} (S/m)$. At 100 kHz, skin depth of copper is found 0.209mm. A 0.15mm diameter copper wire is quite enough to prevent skin effect.

RESUME

Utku KARAKAYA was born in Muğla, in 1981. He completed his higher education in Muğla Anatolian High School, in 1999. He received his Bachelor of Science degree from Yeditepe University Electrical and Electronics Engineering in 2004. Same year, he is accepted to Istanbul Technical University Mechatronics Department for Master programme.